THE AUGUST 1972 SOLAR-TERRESTRIAL EVENTS: SOLAR WIND PLASMA OBSERVATIONS

DEVRIE S. INTRILIGATOR

Physics Department, University of Southern California, Los Angeles, California 90007

Abstract. Solar wind observations associated with the enhanced levels of solar activity in August 1972 are reviewed with an emphasis on recent analyses which more unambiguously characterize the changes in the interplanetary medium. Observations from Pioneer 9 at ~0.8 AU, Pioneer 10 at 2.2 AU, and in the vicinity of Earth are reviewed and reinterpreted in the light of new data. Recent calculations of local shock velocities are reviewed and their implications discussed. These results indicate that contrary to previously published observations there is no significant deceleration of the interplanetary shocks between 0.8 AU and 2.2 AU.

1. Introduction

This paper summarizes many aspects of the observations of the solar wind associated with the August events in 1972. The Pioneer 9 and Pioneer 10 solar wind observations are discussed in detail since these provide the most continuous and unambiguous interplanetary monitoring of the events. Furthermore, the location of these spacecraft with respect to the first series of solar flares was particularly suitable for the study of the radial evolution of the flare associated plasma as it propagated outward through the interplanetary medium.

In Section 2 of this paper there is a brief discussion of the solar flares and the geometry of the flares and the Pioneer 9 and Pioneer 10 locations. In Section 3 there is a discussion of the general Pioneer 9 solar wind plasma observations, the Pioneer 9 shock identifications, and a comparison with simultaneous interplanetary magnetic field observations. Section 4 contains a discussion of the general Pioneer 10 solar wind plasma observations, the Pioneer 10 shock identifications, and a comparison of simultaneous Pioneer 10 plasma and magnetic field observations. In Section 5 the solar wind observations in the vicinity of the Earth are briefly summarized. The Rankine-Hugoniot analysis using the Pioneer 9 solar wind plasma and magnetic field observations of the August events is discussed in Section 6. The calculated shock speeds associated with the Pioneer 9 and Pioneer 10 observations are reviewed in Section 7. In Section 8 the Pioneer 9/Pioneer 10 shock associations are summarized. Estimates of the thickness of some of the shocks are presented in Section 9. The next section briefly summarizes other studies and some conjectures on the dynamics of the evolution of these events with increasing heliocentric distance.

2. Flare and Spacecraft Locations

In early August 1972 there were two 2B solar flares which were followed by two 3B solar flares. The first column in Table I summarizes many of the specifics of these

Space Science Reviews **19** (1976) 629–660.

four flares including the times of onset of activity, the times of maximum activity, and the location of the flare sites. These solar data were obtained from World Data Center A, UAG-28. These flares occurred in McMath Plage 11976 during the descending phase of the solar cycle (solar cycle 20) as indicated in Figure 1. The smoothed sunspot numbers for solar cycles 18 and 19 are also included in Figure 1. This figure emphasizes the similarity in the resurgence of solar activity in the declining phase of each of these solar cycles.

TABLE I

Summary of August events

Location:	Sun	Pioneer 9	Earth	Pioneer 10
Event	Hα Flare 2B	Forward	Forward	Forward
	McMath Plage 11976	Shock	Shock	Shock
	N13° E35°	$S_1(9)$	$S_1(E)$	$S_1(10)$
Time	2 August (Day 215)	3 August (Day 216)	4 August (Day 217)	6 August (Day 219)
	Start 0316 UT	<0430 UT	0120 UT	1520 UT
	End 0800 UT			
	Max 0327 UT			
	0410 UT			
	0515 UT			
	0739 UT			
Event	Hα Flare 2B	Forward	Forward	Reverse
	McMath Plage 11976	Shock	Shock	Shock
	N13° E27°	$S_2(9)$	$S_2(E)$	$S_2(10)$
Time	2 August (Day 215)	3 August (Day 216)	4 August (Day 217)	9 August (Day 222)
	Start 1958 UT	1117 UT	0221 UT	1540 UT
	End 2355 UT			
	Max 2023 UT			
	2058 UT			
Event	Hα Flare 3B	Forward	Forward	Forward
	McMath Plage 11976	Shock	Shock	Shock
	N14° E08°	$S_3(9)$	$S_3(E)$	$S_3(10)$
Time	4 August (Day 217)	4 August (Day 217)	4 August (Day 217)	13 August (Day 226)
	Start 0620 UT	2323 UT	2054 UT	0300 UT
	End 1000 UT			
	Max 0635 UT			
Event	Hα Flare 3B	Forward	Forward	
	McMath Plage 11976	Shock	Shock	
	N14° W36°	$S_4(9)$	$S_4(E)$	
Time	7 August (Day 220)	9 August (Day 222)	8 August (Day 221)	
	Start 1443 UT	0707 UT	2354 UT	
	End 1730 UT			
	Max 1500 UT			
	1527 UT			

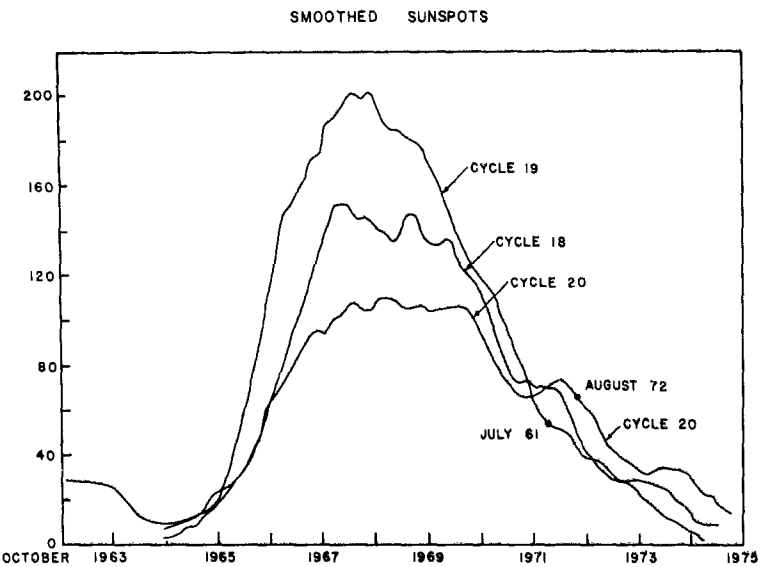

Fig. 1. Solar cycles 18, 19, and 20 with solar cycles 18 and 19 superimposed on solar cycle 20. For solar cycle 18 the beginning of February 1944 was placed on October 1964 and for solar cycle 19 the beginning of April 1954 was placed on October 1964.

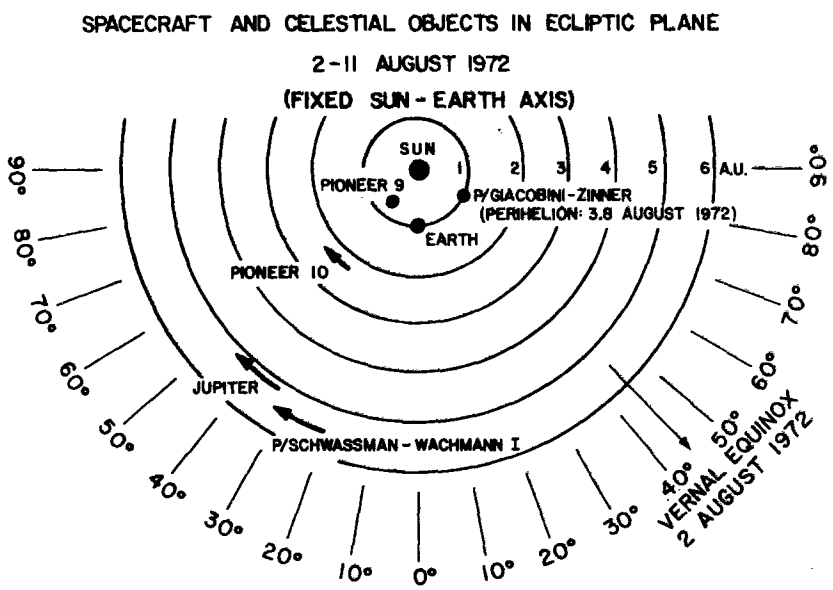

Fig. 2. Ecliptic plane projection of spacecraft and celestial objects within 6 AU in early August 1972.

Figure 2, adapted from Dryer *et al.*, 1975a, shows the ecliptic projections of the locations in early August 1972 of Pioneer 9, Pioneer 10, comet P/Schwassmann-Wachmann I and comet P/Giacobini-Zinner relative to a fixed Sun–Earth axis. In early August 1972, the Pioneer 9 and Pioneer 10 spacecraft were at heliocentric distances of ~0.8 AU and 2.2 AU, respectively, approximately 45° east of the Earth's solar longitude. Pioneer 9 was located approximately $11–13 \times 10^5$ km north of the ecliptic plane during this time and Pioneer 10 was located approximately $11–12 \times 10^6$ km south of the ecliptic plane.

Referring again to Table I, the last three columns indicate, respectively, the sequence of times of observation at Pioneer 9, Earth, and Pioneer 10 of the interplanetary shocks. Throughout this paper we will use the convention of numbering sequentially the shocks at each location indicating in parentheses the location. Therefore, $S_1(9)$ denotes the first shock observed at Pioneer 9, $S_1(E)$ denotes the first shock observed at Earth, and $S_1(10)$ denotes the first shock observed at Pioneer 10.

3. Pioneer 9 Observations

Figure 3 is from Intriligator (1976a) and summarizes the solar wind plasma parameters observed in early August 1972 at Pioneer 9. The Pioneer 9 plasma data in this figure and subsequent figures (also from this reference) were obtained from the NASA Ames Research Center solar wind plasma analyzer, John Wolfe is the principal investigator. Figure 4 presents higher time resolution data of the solar wind proton speed and magnetic field magnitude at the time of the first shock $S_1(9)$ observed at Pioneer 9. The

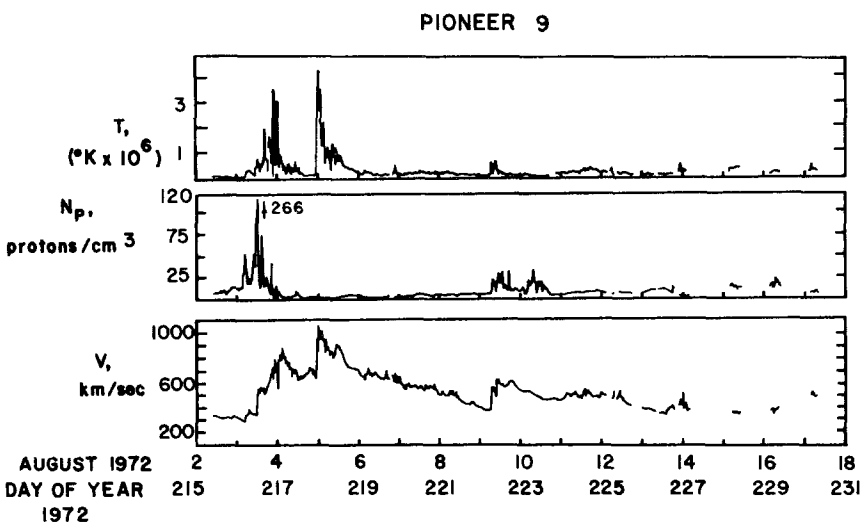

Fig. 3. Solar wind plasma proton observations obtained on Pioneer 9 ~0.8 AU during the period 2 August (Day 215) to 18 August (Day 231), 1972 by the NASA Ames Research Center Plasma Analyzer. The solar wind proton streaming speed, V; the solar wind proton number density, N_p; and the solar wind proton temperature, T, are shown.

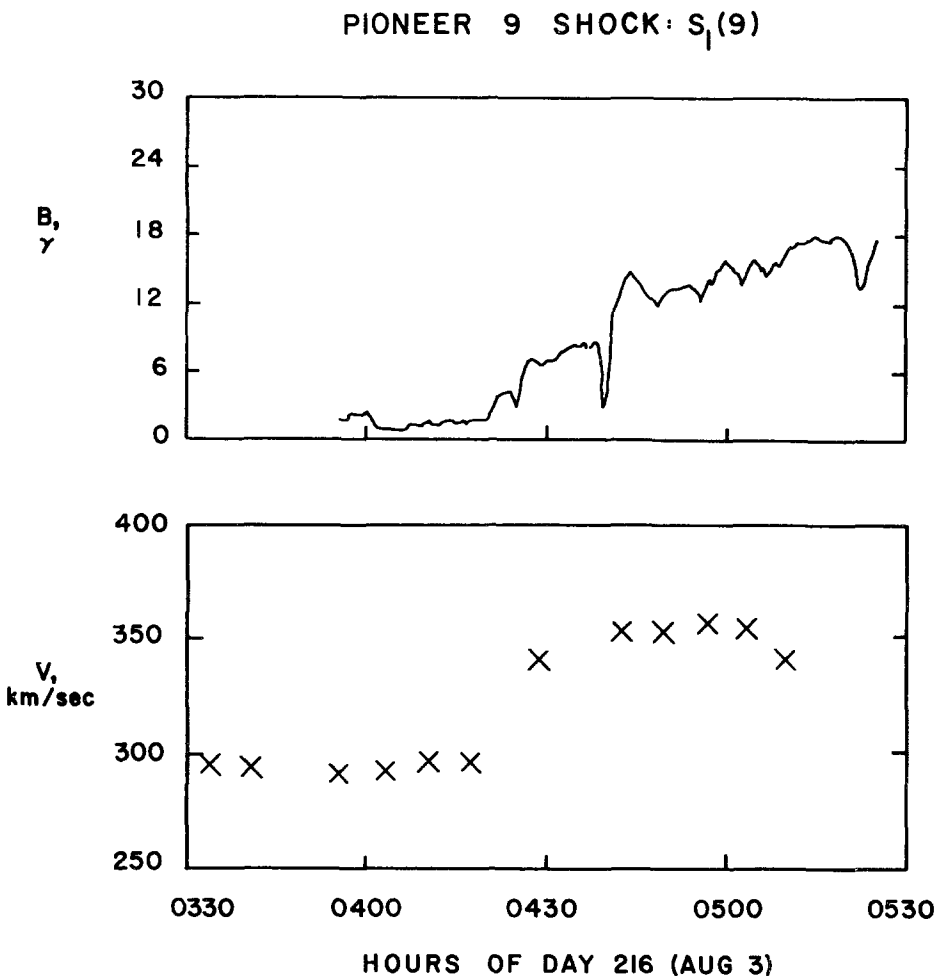

Fig. 4. Simultaneous observations of the solar wind proton speed, V, and the magnetic field magnitude, B, in the vicinity of the Pioneer 9 forward shock $S_1(9)$. The $\times$'s, in this and subsequent figures, are the least squares analyzed values of the solar wind proton speed obtained by the NASA Ames Research Center plasma analyzer. The magnetic field data in this figure and Figures 6, 8 and 10 were obtained by the Pioneer 9 magnetometer. Intriligator (1976a) has noted that the data indicate that there is a jump in the solar wind proton speed before 0430 UT implying the passage of the shock before 0430 UT rather than at ~0440 UT as had been previously reported by others.

magnetic field data were obtained by the NASA Ames Research Center magnetometer, Charles Sonett is the principal investigator. The solar wind proton speed points in this and subsequent figures were obtained from the NASA Ames Research Center least squares data reduction program that obtains the plasma parameters of the plasma distribution function by iterating the data with the specific instrument response function obtained in the prelaunch calibration of the instrument in the Plasma Calibration Facility at NASA Ames Research Center. Intriligator (1976a) was the first to point out that previously the time of the first shock reaching Pioneer 9 had

been incorrectly reported as 0440 UT. It is clear in the higher time resolution data shown in Figure 4 that there is a sharp increase in the solar wind proton speed before 0430 UT. Figure 4 also indicates that the increase in speed before 0430 UT corresponds to an enhancement in the magnetic field magnitude. The identification of the time of arrival of this first shock $S_1(9)$ at Pioneer 9 is further discussed in Intriligator (1976a) with the use of ion energy spectra. Figure 5, taken from this paper, shows ion energy spectra obtained on Day 216 (3 August) at approximately 0417 UT and 0428 UT. In this figure and subsequent figures of this type, the flux shown is the peak ion flux in ions per square centimeter per second for each energy per unit charge channel. The speed shown is the proton speed obtained from converting the energy associated with the energy per unit charge channel to the comparable proton speed in kilometers per second. The peak in the ion energy spectrum obtained at ~0417 UT was measured before the arrival of the first shock $S_1(9)$ at Pioneer 9. The solar wind proton speed associated with this peak is $\sim 290\ km\ s^{-1}$. The peak in the ion energy spectrum obtained around 0428 UT was measured after the arrival of $S_1(9)$ at Pioneer 9. The solar wind proton speed associated with this peak is $\sim 340\ km\ s^{-1}$. Intriligator (1976a) also noted the enhanced intensity of the second peak in the 0428 UT spectrum as

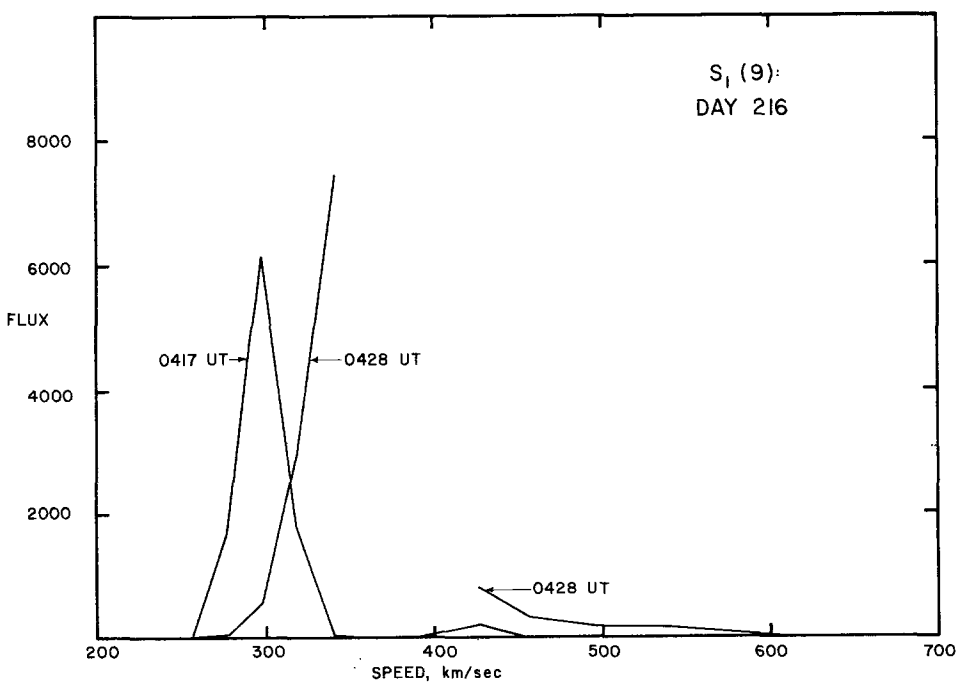

Fig. 5. Differential Ion Energy per Unit Charge Spectra. The flux shown is the peak ion flux for each energy per unit charge channel measured in ions per square centimeter per second in that channel. The speed shown is the proton speed obtained from converting the energy associated with the energy per unit charge channel to the comparable proton speed. The ion energy spectrum measured at 0417 UT was obtained before the passage of $S_1(9)$. The ion energy spectrum measured at 0428 UT peaks at a higher solar wind proton speed implying that it was measured after the passage of $S_1(9)$.

compared with the intensity of the second peak in the 0417 UT spectrum. The second peak in the 0417 spectrum is associated with the alpha particle intensity. The enhancement of this peak in the 0428 UT spectrum is most likely indicative of an increase in the number of alpha particles in the solar wind and also an enhanced high energy tail associated with the solar wind proton energy distribution function. The increase in the solar wind proton speed from 290 km s^{-1} at ~0417 UT to 340 km s^{-1} at ~0428 UT and the general change in the shape of the ion energy spectra between ~0417 UT and ~0428 UT have led Intriligator (1976a) to conclude that $S_1(9)$ arrived at Pioneer 9 before 0430 UT (e.g., ~0428 UT) rather than at 0440 UT as had been previously reported by others.

Figure 6 is similar in format to Figure 4, and shows the arrival of the second shock $S_2(9)$ at Pioneer 9. In this figure the higher time resolution data indicate that the increase in the solar wind proton speed occurred between ~1100 UT and ~1130 UT.

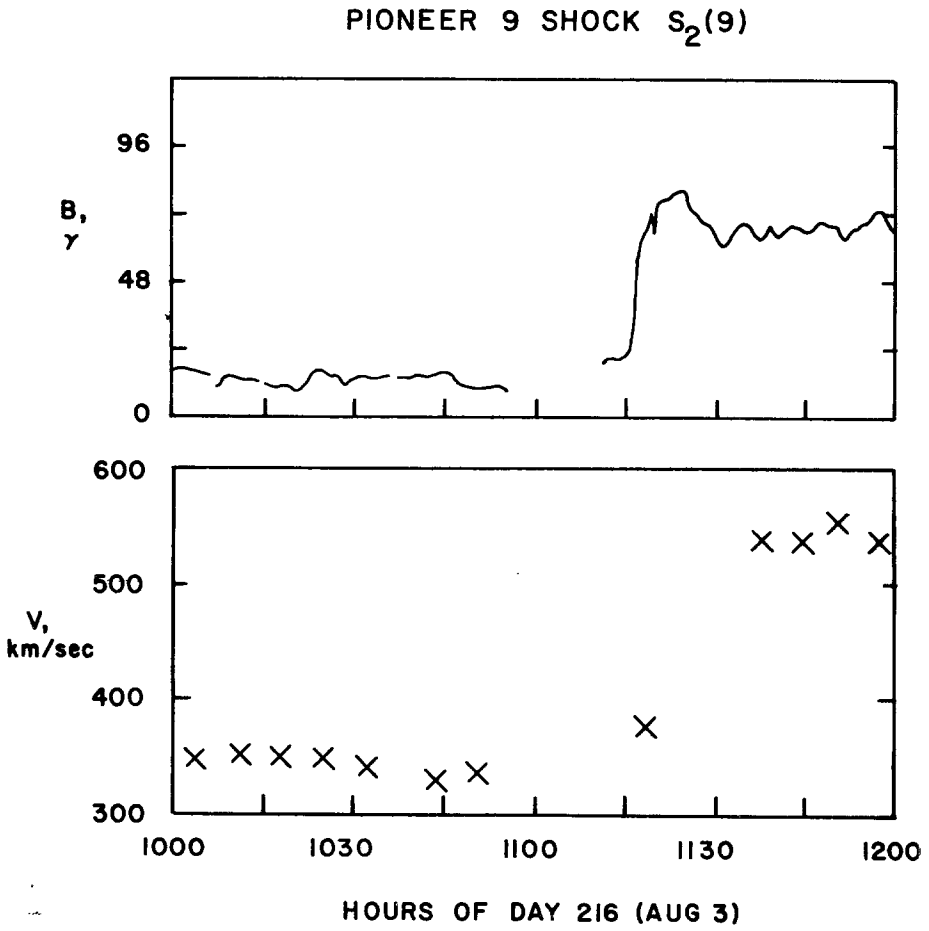

Fig. 6. Simultaneous observations of the solar wind proton speed, V, and the magnetic field magnitude, B, in the vicinity of the Pioneer 9 forward shock $S_2(9)$.

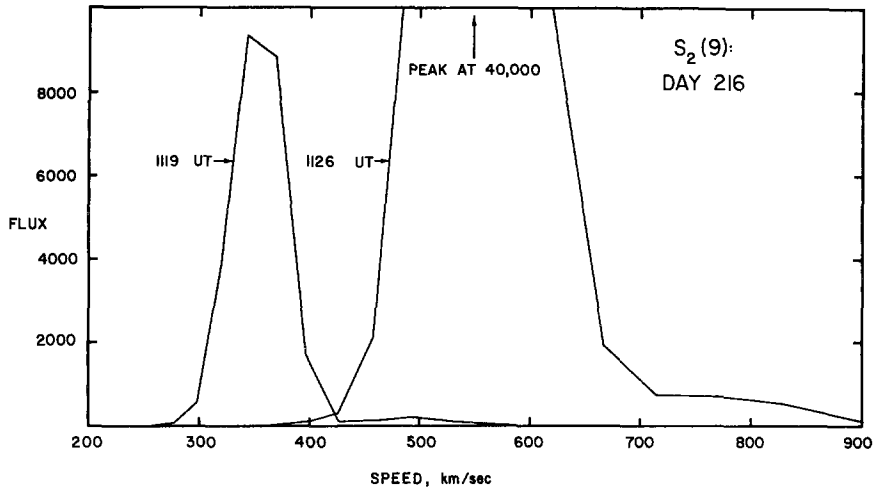

Fig. 7. Differential Ion Energy per Unit Charge Spectra measured at Pioneer 9 on Day 216 (see caption of Fig. 5 and text for an explanation of the format). The ion energy spectrum obtained at 1126 UT has a much higher intensity and peaks at a substantially higher solar wind proton speed than the ion energy spectrum obtained earlier at 1119 UT.

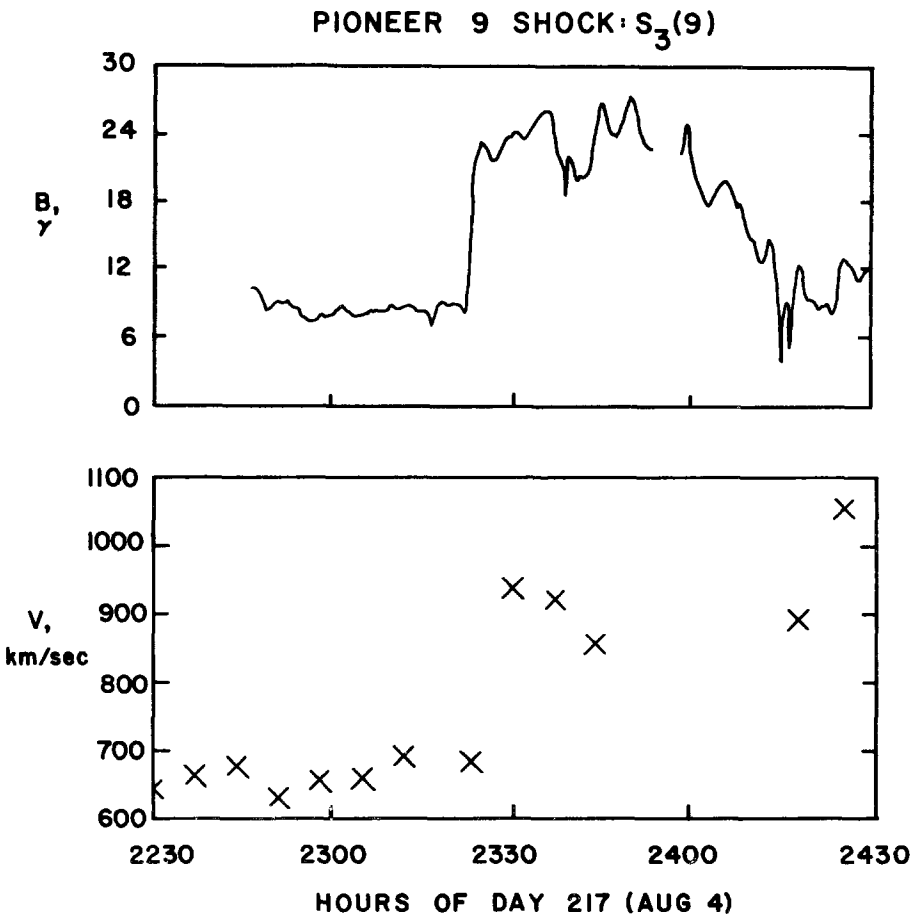

Fig. 8. Simultaneous observations of the solar wind proton speed, V, and the magnetic field magnitude. B, in the vicinity of the Pioneer 9 forward shock $S_3(9)$.

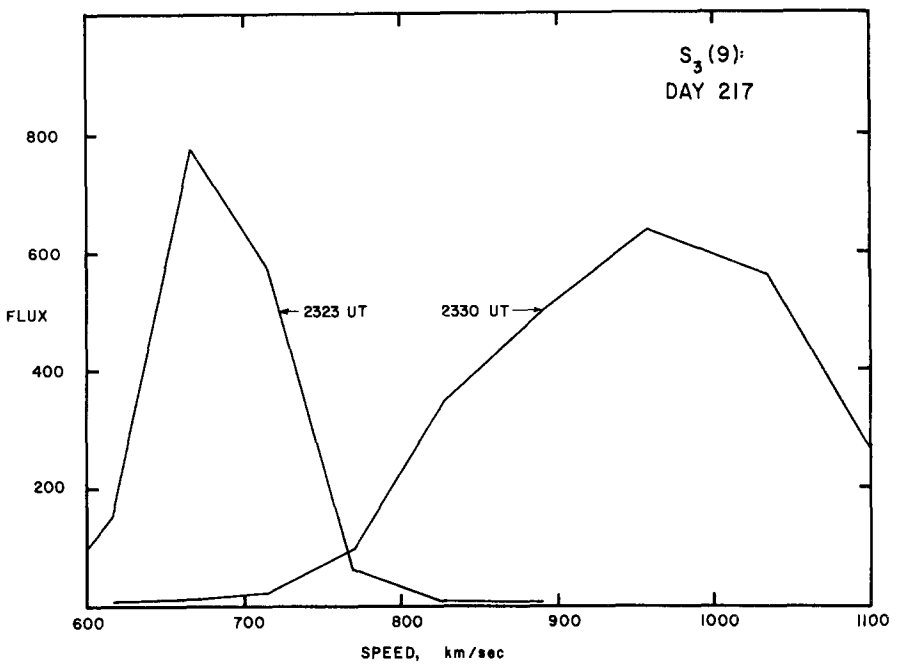

Fig. 9. Differential Ion Energy per Unit Charge Spectra measured at Pioneer 9 on Day 217 (see caption of Fig. 5 and text for an explanation of the format). The ion energy spectrum obtained at 2330 UT peaks at a substantially higher solar wind proton speed than the spectrum obtained at 2323 UT. The temperature (as indicated by the full width at half maximum) of the spectrum measured ~2330 UT is also higher.

The marked increase in the magnetic field magnitude during this time is also clearly shown. The identification of the time of arrival of shock $S_2(9)$ at Pioneer 9 is further discussed in Intriligator (1976a) with the use of ion energy spectra. Figure 7, which is taken from this paper, shows ion energy spectra obtained on Day 216 (3 August) at approximately 1119 UT and 1126 UT. This figure emphasizes the drastic change in the solar wind distribution function as a result of the arrival of $S_2(9)$. Figure 7 indicates the large increase in solar wind proton speed from the value of 350 km s^{-1} associated with the peak of the 1119 UT energy spectrum to a speed of 550 km s^{-1} associated with the peak of the 1126 UT energy spectrum. Figure 7 also shows the substantial increase in intensity associated with the 1126 UT energy spectrum.

Figure 8 shows the simultaneous solar wind proton speed data and magnetic field magnitude data associated with the arrival of the third shock $S_3(9)$ at Pioneer 9. There is a definite increase in the solar wind speed and magnetic field magnitude at ~2330 UT. Figure 9 shows the changes in the solar wind ion energy spectrum associated with the arrival of $S_3(9)$. This figure is similar in format to Figures 5 and 7, although the vertical scale in Figure 9 has been expanded to more fully show the slope of these ion energy spectra and the horizontal scale now covers the range from 600 km s^{-1} to 1100 km s^{-1}. The ion energy spectra in Figure 9 show the large shift

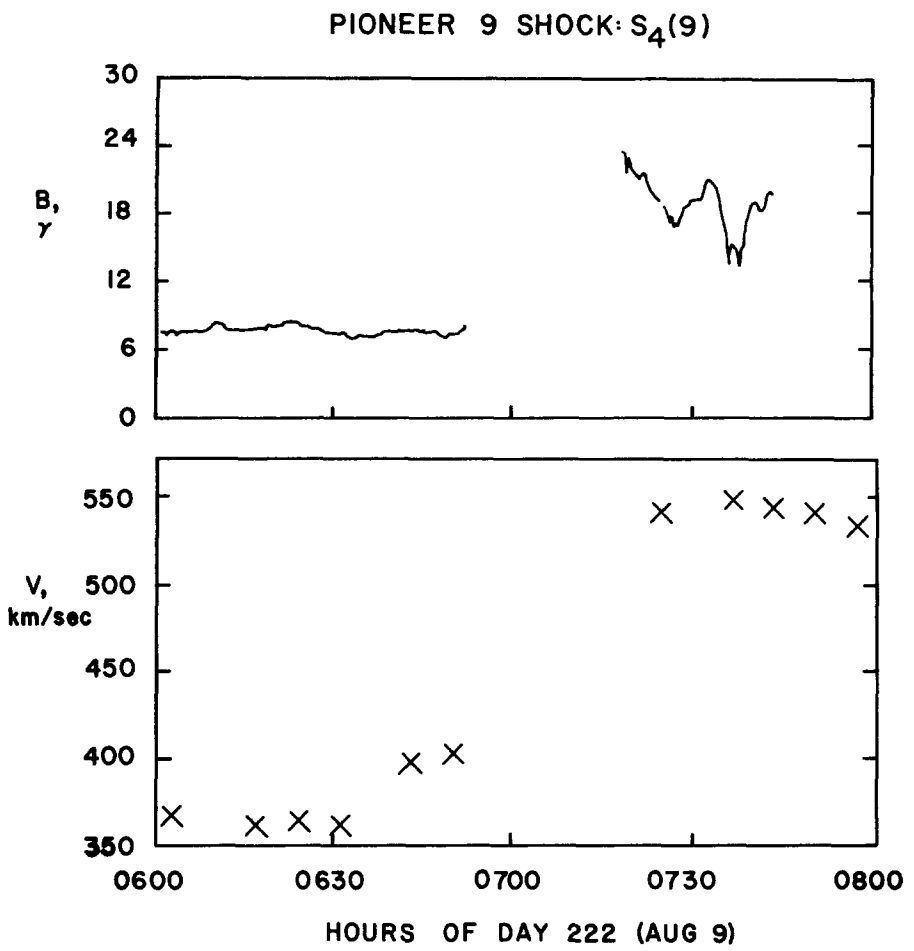

Fig. 10. Simultaneous observations of the solar wind proton speed, V, and the magnetic field magnitude, B, in the vicinity of the Pioneer 9 forward shock $S_4(9)$.

in the peak of the solar wind ion energy spectrum from a solar wind proton speed of 650 km s^{-1} at 2323 UT to a speed of 920 km s^{-1} at 2330 UT. Intriligator (1976a) noted the general enhanced intensity of the ion energy spectrum at 2330 UT and the extended high energy tail associated with this spectrum.

The data associated with $S_4(9)$ are shown in Figure 10. The large increase in both the plasma proton speed and the magnetic field magnitude occur during the data gap ~0700 UT. The ion energy spectra obtained just before and after this data gap are shown in Figure 11. This figure shows the increase in the solar wind proton speed associated with the peak of the ion energy spectrum from a value of 400 km s^{-1} in the spectrum obtained at 0650 UT to 540 km s^{-1} in the spectrum measured at 0725 UT after the data gap. The increased intensity and enhanced high energy tail of the ion energy spectrum measured at 0725 UT after the arrival of $S_4(9)$ as compared to that

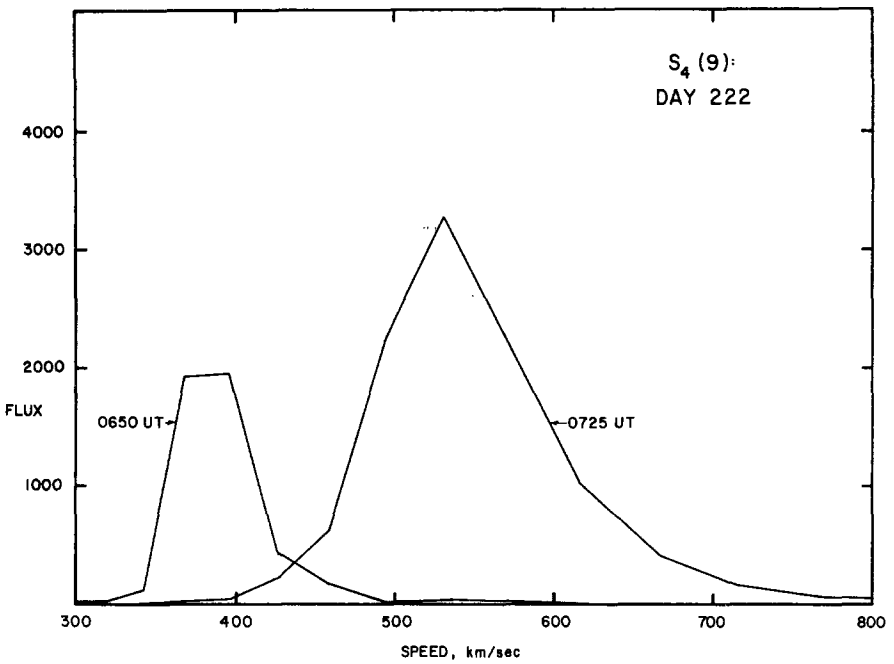

Fig. 11. Differential Ion energy per Unit Charge Spectra measured at Pioneer 9 on Day 222 (see caption of Fig. 5 and text for an explanation of the format). The ion energy spectrum measured at 0650 UT was obtained before the passage of $S_4(9)$. The ion energy spectrum measured at 0725 UT shows a higher peak speed and temperature implying its association with the passage of $S_4(9)$.

measured at 0650 UT before the arrival of $S_4(9)$, are similar to those shown above in Figures 5, 7, and 9 for the ion energy spectra associated with the arrivals of $S_1(9)$, $S_2(9)$, and $S_3(9)$, respectively.

Analyses of the Pioneer 9 solar wind plasma and magnetic field data presented above have led to the identification (Intriligator, 1976a; Smith, 1976) that each of the four shocks $S_1(9)$, $S_2(9)$, $S_3(9)$, and $S_4(9)$ are fast forward shocks. These results confirm the earlier identifications by Mihalov *et al.* (1974) and Dryer *et al.* (1976). The Rankine-Hugoniot analyses of the shocks are discussed in Section 6. The calculations of the local shock speeds at Pioneer 9 are discussed in Section 7 and the shock associations between Pioneer 9 and Pioneer 10 are discussed in Section 8. A discussion of the plasma wave measurements and power spectral analyses is included in Section 10.

4. Pioneer 10 Observations

Figure 12 is from Intriligator (1976a) and summarizes the solar wind plasma parameters observed in early August 1972 at Pioneer 10. The Pioneer 10 plasma data in this figure and subsequent Figures 13–18 (also from this reference) were obtained from the NASA Ames Research Center solar wind plasma analyzer (Intriligator and Wolfe, 1976). John Wolfe is the principal investigator of this experiment. Figure 13

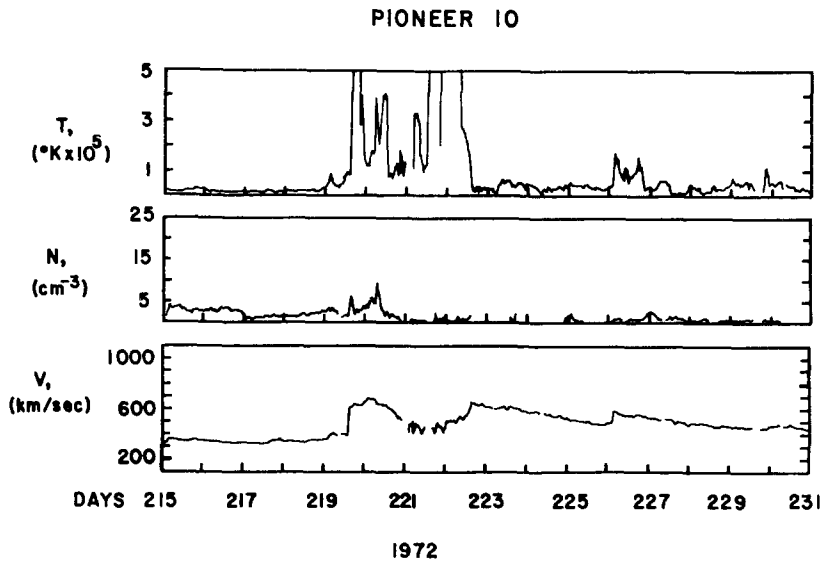

Fig. 12. Solar wind plasma observations obtained on Pioneer 10 at 2.2 AU during the period 2 August (Day 215) to 18 August (Day 231), 1972 by the NASA Ames Research Center Plasma Analyzer. The solar wind proton streaming speed, V; the solar wind proton number density, N; and the solar wind proton temperature, T, are shown.

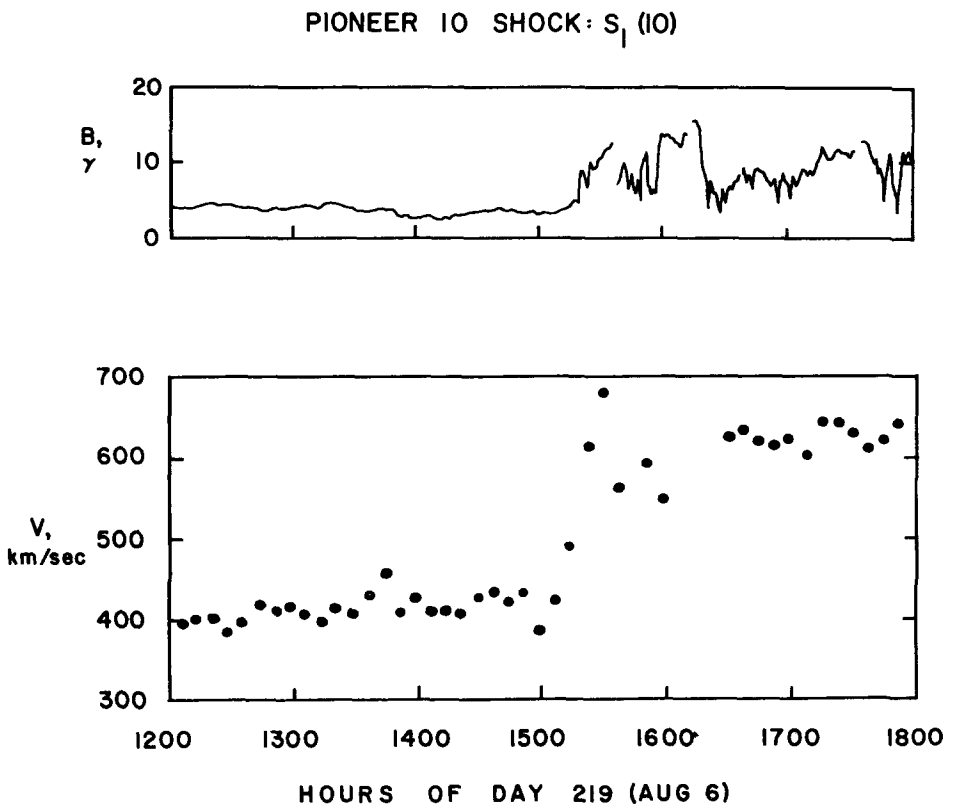

Fig. 13. Simultaneous observations of the solar wind proton speed, V, and the magnetic field magnitude, B, in the vicinity of the Pioneer 10 forward shock $S_1(10)$. The dots, in this figure and subsequent figures, are the least squares analyzed values of the solar wind proton speed obtained by the NASA Ames Research Center Plasma Analyzer. The magnetic field data in this and subsequent figures were obtained by the Vector Helium Magnetometer on Pioneer 10.

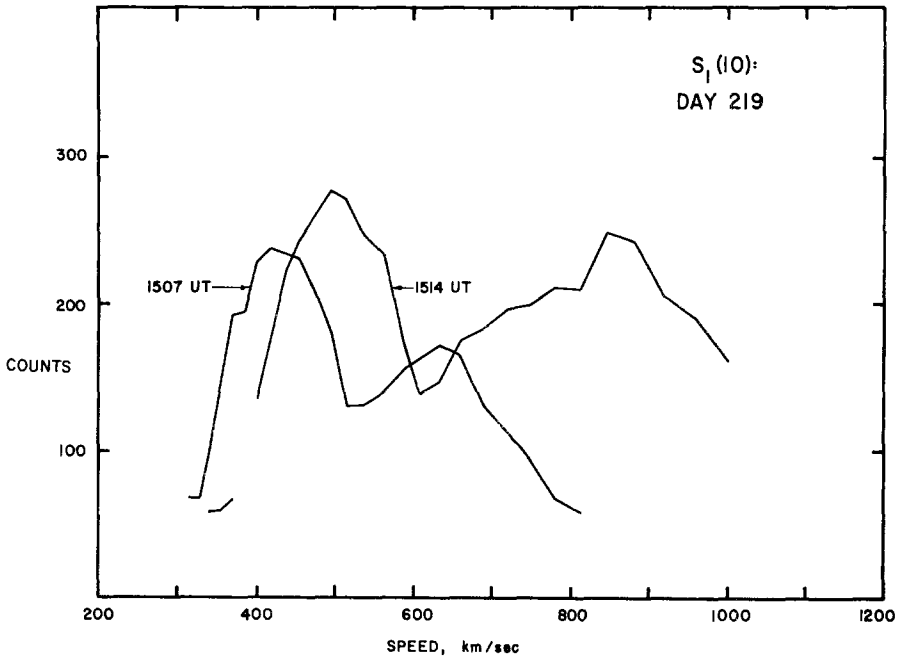

Fig. 14. Differential Ion Energy per Unit Charge Spectra. The count shown is the peak ion count for each energy per unit charge channel measured in ions per square centimeter per second in that channel. The speed shown is the proton speed obtained from converting the energy associated with the energy per unit charge channel to the comparable proton speed. The ion energy spectrum obtained at 1514 UT peaks at a higher solar wind proton speed than the 1507 UT spectrum. The 1514 UT spectrum has a more 'ragged' shape possibly implying that it is time aliased (Intriligator, 1976a).

presents higher time resolution data of the solar wind proton speed and magnetic field magnitude at the time of the first shock $S_1(10)$ observed at Pioneer 10. The Pioneer 10 magnetic field data in this figure and subsequent figures were obtained by the Helium Vector Magnetometer on Pioneer 10 (Smith *et al.*, 1974). Edward J. Smith is the principal investigator of this experiment. The solar wind proton speed points in this figure and subsequent figures were obtained from the NASA Ames Research Center least squares data reduction program that obtains the plasma parameters of the plasma distribution function by iterating the data with the specific instrument response function obtained in the prelaunch calibration of the instrument in the Plasma Calibration Facility at NASA Ames Research Center. Figure 13 shows the increase in the solar wind proton speed ~1500 UT and the jump in the magnetic field magnitude. In the ion energy per unit charge spectra obtained at ~1507 UT and subsequent ion energy spectra of this type, the flux shown is the peak ion flux in ions per square centimeter per second for each energy per unit charge channel. The speed shown is the proton speed obtained from converting the energy associated with the energy per unit charge channel to the comparable proton speed in kilometers per second. In Figure 14 the peak in the ion energy spectrum measured at ~1507 UT was

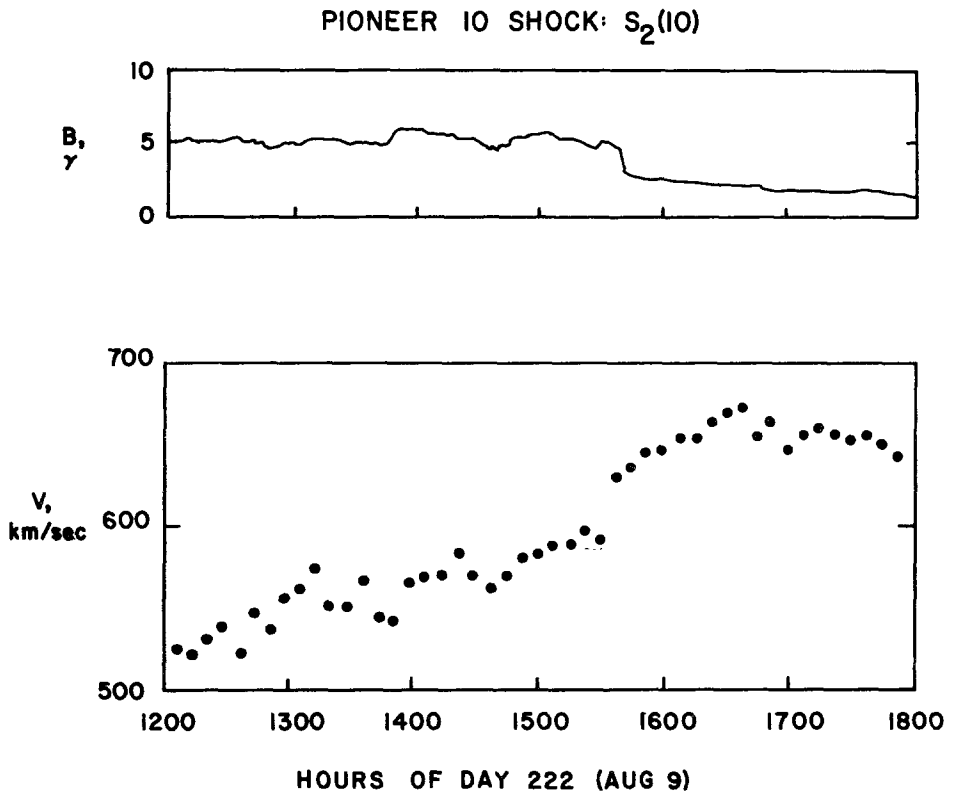

Fig. 15. Simultaneous observations of the solar wind proton speed, V, and the magnetic field magnitude B, in the vicinity of the Pioneer 10 reverse shock S_2(10).

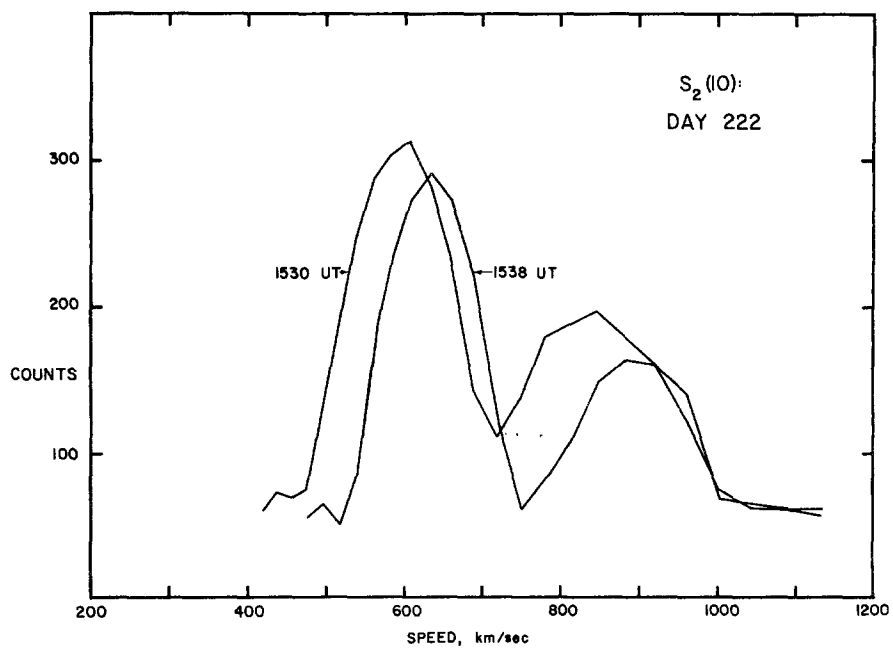

Fig. 16. Differential Ion Energy per Unit Charge Spectra. This figure is similar in format to Fig. 14. The ion energy spectrum measured at 1538 UT peaks at a higher solar wind proton speed than the earlier (1530 UT) spectrum.

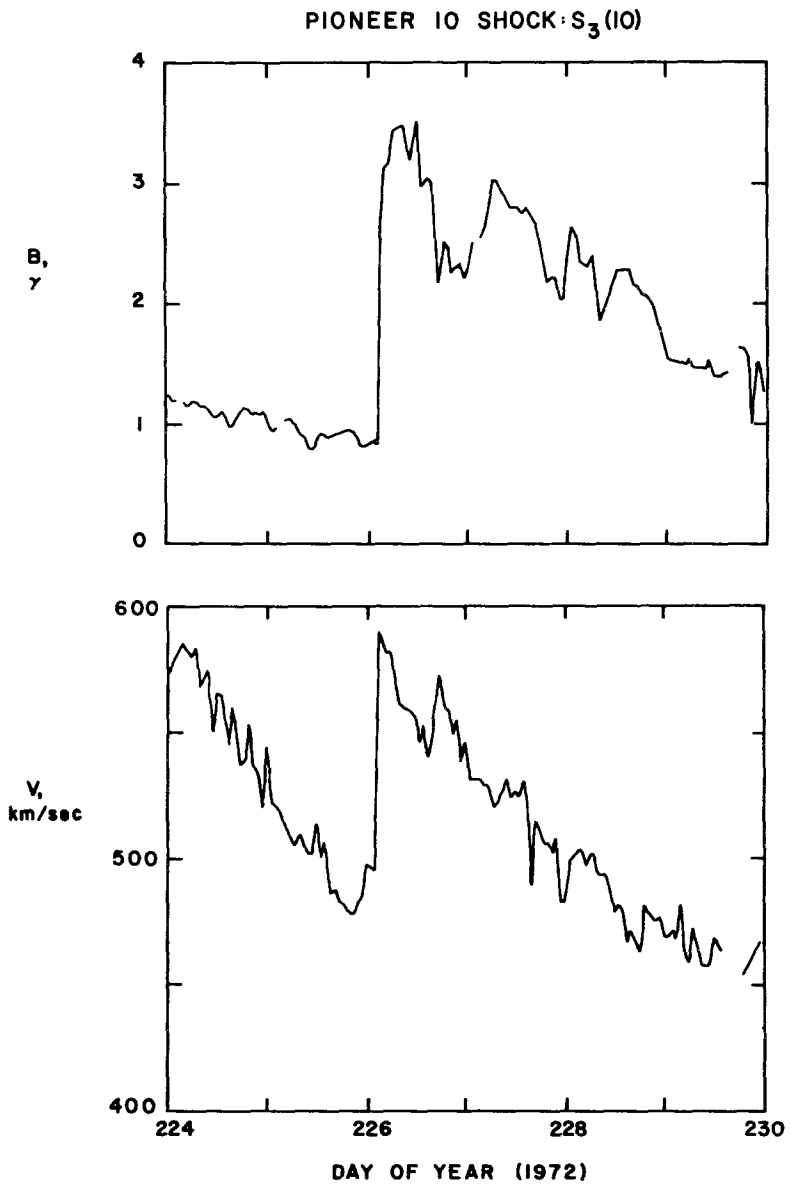

Fig. 17. Simultaneous observations of the solar wind proton speed, V, and the magnetic field magnitude, B, from Day 224 to Day 230. The simultaneous jump in these parameters on Day 226 is associated with the passage at Pioneer 10 of the forward shock $S_3(10)$.

measured before the arrival of the first shock $S_1(10)$ at Pioneer 10. The solar wind proton speed associated with this peak is ~ 400 km s^{-1}. The peak in the ion energy spectrum obtained at ~ 1514 UT was measured after the arrival of $S_1(10)$ at Pioneer 10. In Intriligator (1976a) ion energy spectra obtained at ~ 1530 UT and ~ 1538 UT are also presented, and it is noted that the ion spectra obtained at 1514 UT, that is

shown in Figure 14, has a generally more 'ragged' shape than the others possibly implying that it is time aliased.

Figure 15 shows the arrival of the second shock $S_2(10)$ at Pioneer 10. In this figure the higher time resolution data indicate that there is a gradual increase in solar wind proton speed on Day 222 (9 August) between ~1200 UT and 1640 UT. The higher time resolution magnetic field data in the top panel of Figure 15 indicate that unlike the other shocks at Pioneer 9 and Pioneer 10, there is a sharp drop in magnetic field magnitude at ~1550 UT. This drop in magnetic field magnitude has led to the identification of $S_2(10)$ as a reverse shock. The ion energy spectra associated with the arrival of $S_2(10)$ at Pioneer 10 are shown in Figure 16. This figure shows the increase in the solar wind proton speed between 1530 UT (Day 222) and 1538 UT. In Figure 17 Pioneer 10 measurements of the solar wind proton speed and the simultaneous magnetic field magnitude are shown for Days 224–230. The sharp increase in the solar wind speed at the beginning of Day 226 is accompanied by a dramatic jump in the magnetic field magnitude. The change in the solar wind ion energy spectra due to the arrival of $S_3(10)$ at Pioneer 10 is shown in Figure 18. The ion energy spectrum measured at ~0230 UT was obtained before the arrival of $S_3(10)$. This ion energy spectrum peaks at a solar wind proton speed of ~500 km s^{-1}. The ion energy spectrum measured

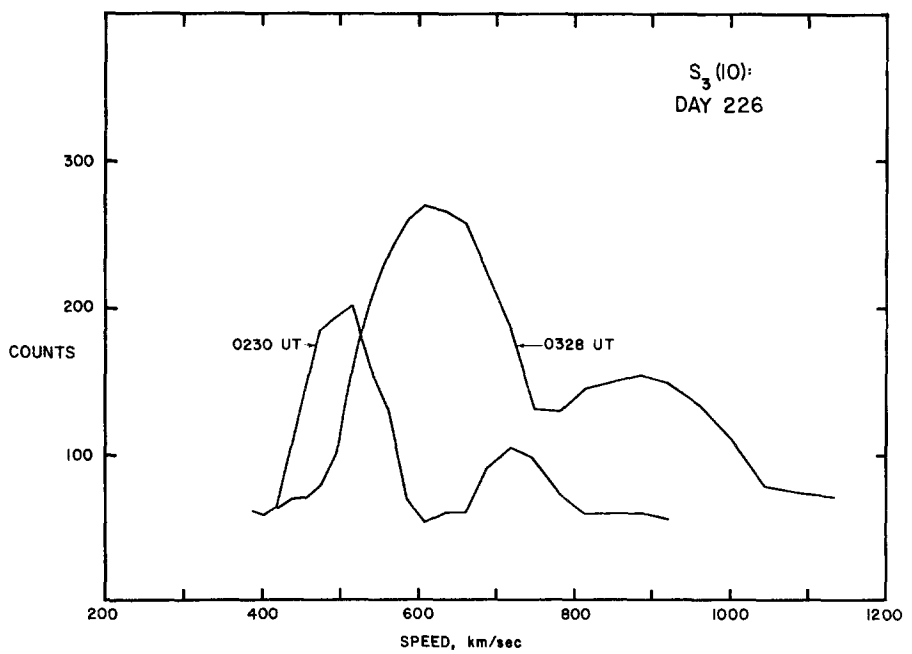

Fig. 18. Differential Ion Energy per Unit Charge Spectra (see caption of Fig. 14 for an explanation of the format). The ion energy spectrum measured at 0230 UT was obtained before the passage of $S_3(10)$. The 0328 UT spectrum was obtained after the passage of $S_3(10)$ since it peaks at a higher solar wind proton speed, shows enhanced intensity, and a higher temperature as indicated by the full width at half maximum.

at ~0328 UT was obtained after the arrival of $S_3(10)$ at Pioneer 10. In contrast to the earlier ion energy spectrum, the one obtained at ~0328 UT peaks at a solar wind proton speed of ~600 km s^{-1}, and shows an enhanced intensity of the solar wind proton and alpha particles and also shows evidence of a high energy tail to the solar wind proton (and perhaps alpha particle) distribution function.

Analysis of the Pioneer 10 solar wind plasma and magnetic field data presented above have led to the identification (Intriligator, 1976a; Smith, 1976) of $S_1(10)$ and $S_3(10)$ as fast forward shocks and $S_2(10)$ as a reverse shock. In Section 7 there is a discussion of the calculations of the local shock speeds associated with these shocks. The shock association between Pioneer 9 and Pioneer 10 and the implications of these identifications are reviewed in Section 8. Estimates of the thickness of $S_1(10)$ and $S_2(10)$ are reviewed in Section 9. Power spectral analyses of the Pioneer 10 data are briefly discussed in Section 10.

5. Near-Earth Observations

Solar wind observations associated with the August events in the vicinity of the earth have been reported by Cattaneo *et al.* (1974), Zastenker *et al.* (1975) and Vaisberg and Zastenker (1976).

Figure 19a is adapted from Vaisberg and Zastenker (1976) and shows measurements of the solar wind speed (based on hourly averages) obtained on Prognoz-1 and Prognoz-2. The Prognoz satellites had highly eccentric orbits with apogee ~200 000 km, perigree ~1000 km and an orbital inclination of ~65° (Vaisberg and Zastenker, 1976) thereby allowing them to spend a large fraction of the orbital period in the solar wind. Column 3 in Table I lists in the vicinity of the earth the sequence of arrival of the four shocks in early August 1972. In Figure 19a the jumps can be clearly seen in the solar wind speed on Day 217 (4 August) at ~0100 UT, ~0200 UT, and ~2100 UT which are associated with the arrival of the first three shocks $S_1(E)$, $S_2(E)$, and $S_3(E)$ in the vicinity of Earth. The higher solar wind speed following the data gap on Day 221 (8 August) is associated with the arrival of the fourth shock $S_4(E)$.

Figure 19b is similar to Figure 19a but some additional data have been superimposed on the Prognoz-1 and Prognoz-2 measurements. Following Vaisberg and Zastenker (1976), the HEOS-2 plasma speeds have been added. The dots are the solar wind speed measurements and the dashed lines are the measurements of the plasma speed in the magnetosheath. In Figure 19b the continuous histogram indicates the three-hourly value of the K_p index for geomagnetic activity recorded at ground stations. There is a general tendency for the arrival of interplanetary shocks to produce increases in geomagnetic activity as indicated by the K_p index (Intriligator, 1973) and sudden commencements. Figure 19b also indicates, however, that there are several times when the increases in the K_p index are not accompanied by the arrival of shocks or large increases in the solar wind speed.

Croft (1975) has published data on the electron content along the path from Earth

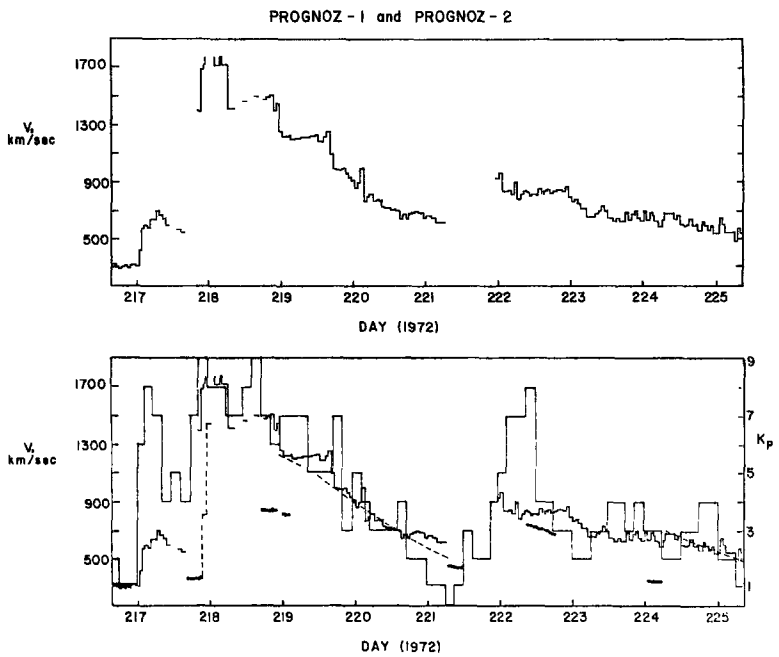

Fig. 19a (upper panel). Solar wind proton speed obtained on satellites Prognoz-1 and Prognoz-2 in August 1972.

Fig. 19b (lower panel). HEOS-2 data and the three-hourly ground based K_p index have been superimposed on the Prognoz data. The dots are the HEOS-2 solar wind speed measurements and the dashed lines are the HEOS-2 measurements of the plasma speed in the magnetosheath. The histogram shows the three hourly K_p index and refers to the scale at the right of the figure.

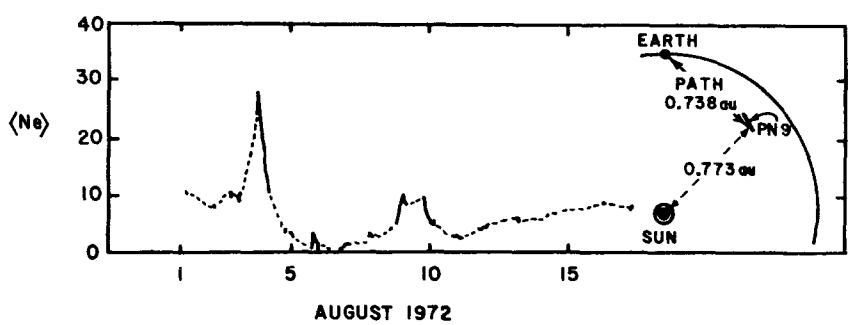

Fig. 20. The normalized average electron density (in electrons cm^{-3}) measured along the radio path from earth to Pioneer 9. The insert at the right indicates the path.

to Pioneer 9 based on measurements with the Stanford dual-frequency system on Pioneer 9. Figure 20 is adapted from Croft (1975) and shows the normalized average electron density (in electrons cm^{-3}) measured along the radio path from Earth to Pioneer 9 in early August 1972. In Figure 20 we have inserted a schematic drawing indicating the specific location of this radio path from Earth to Pioneer 9 during early August 1972. The data in Figure 20 were obtained by taking the estimated electron

content along the entire path from the surface of the Earth to the spacecraft, then subtracting the large contribution from the Earth's ionosphere, and then dividing the remaining electron content by the path length ($\sim 111 \times 10^6$ km). The data in Figure 20 show large variations during this interval of the average electron number density along this path. The data imply first ~ 3 August the presence of higher density regions and then ~ 5, 6 August the virtual evacuation of most electrons from this path.

6. Rankine-Hugoniot Analysis

Dryer *et al.* (1976) have performed extensive calculations of the parameters associated with the four forward shocks at Pioneer 9. Using the simultaneous plasma and magnetic field data they have obtained many important quantities such as the Mach numbers, the plasma betas and the other plasma parameters listed in Table II (which is adapted from Dryer *et al.*, 1976). These quantities have been derived from the use of the Rankine-Hugoniot relations. In this type of analysis (Tidman and Krall, 1971; Lepping and Argentiero, 1971; Dryer *et al.*, 1975b) the magnetohydrodynamic shock jump conditions (Landau and Lifshitz, 1960; Colburn and Sonett, 1966) are derived from the conservation equations and Maxwell's equations, assuming that the solar

TABLE II

Plasma parameters derived from Rankine-Hugoniot analysis (adapted from Dryer *et al.*, 1976)

Plasma parameter	$S_1(9)$	$S_2(9)$	$S_3(9)$	$S_4(9)$
Alfvén Mach No., M_A	4.4	5.1	2.9	3.8
Alfvén Mach No. perpendicular to shock plane, $M_{A\perp}$	10.6	26.8	6.2	3.5
Ordinary Mach No., M	17.3	10.0	39.6	10.3
$\beta_p = 2\mu nkT_p/B^2$	0.16	0.41	0.016	0.24
$\beta_e = 2\mu nkT_e/B^2$	1.90	0.86	0.18	0.008
$\beta_T = \beta_p + \beta_e$	2.06	1.27	0.20	0.25
Angle between shock normal and magnetic field, $\theta_{\mathbf{B},\hat{n}}$	76°	79°	64°	37°
Angle between shock normal and relative velocity, $\theta_{\mathbf{V},\hat{n}}$	54°	74°	16°	43°
Preshock electron temperature, T_e(°K)	2.7×10^5	1.8×10^5	4.3×10^5	0.4×10^5
Postshock electron temperature, T_e'(°K)	3.7×10^5	16.0×10^5	11.0×10^5	7.1×10^5
Preshock proton temperature, T_p(°K)	0.2×10^5	0.9×10^5	0.2×10^5	1.2×10^5
T_p'(°K)	0.9×10^5	3.3×10^5	15.0×10^5	4.5×10^5
Shock velocity in direction (θ, ϕ) of normal, V_S, km s^{-1}	371 (−21°, 203°)	645 (3.5°, 166°)	1096 (−3.8°, 158°)	601 (−26°, 178°)
Shock velocity in radial direction, V_{SR}, km s^{-1}	431	667	1183	672
Ion inertial length, c/ω_{pi}, km	57	29	175	106

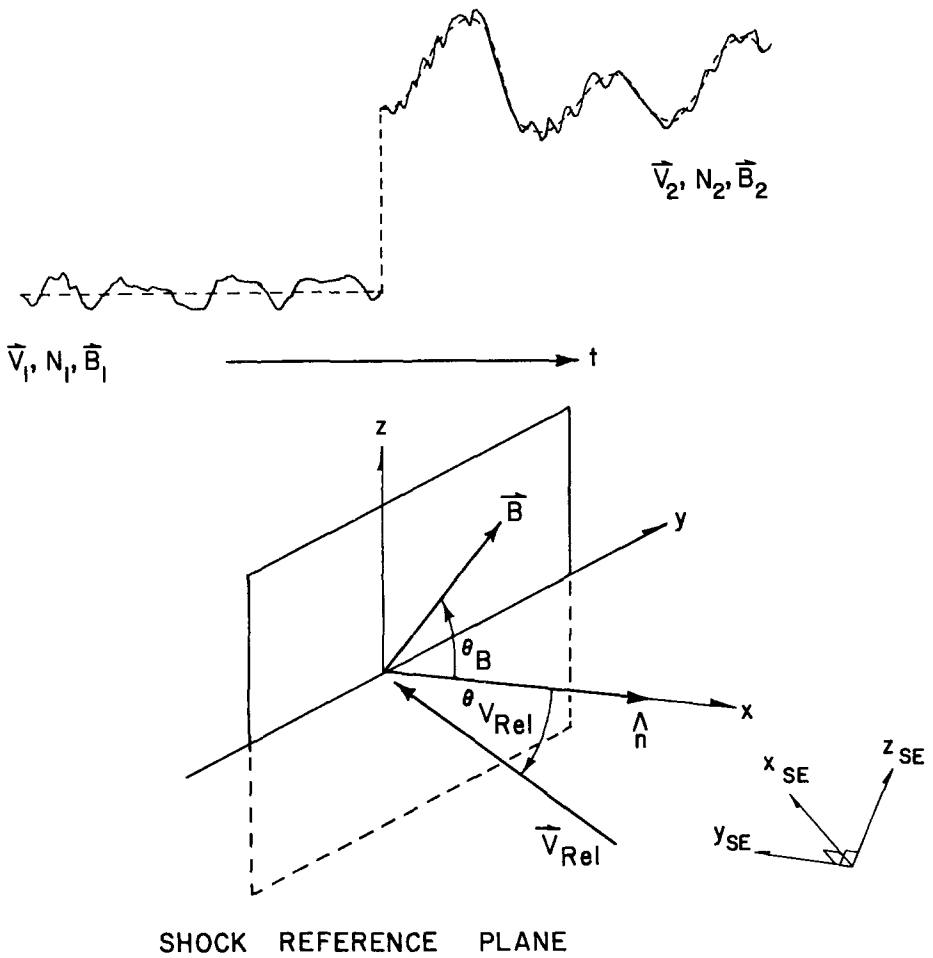

Fig. 21 (upper panel). Conceptual drawing of the interplanetary plasma and magnetic field parameters as a function of (increasing) time. The parameters $\mathbf{V}_1$, N_1, and $\mathbf{B}_1$ characterize the interplanetary medium before the discontinuous jump in the parameters associated with the shock front. The parameters $\mathbf{V}_2$, N_2, and $\mathbf{B}_2$ characterize the interplanetary medium after the time of the shock. (Lower panel) Drawing of the shock reference plane.

wind behaves as an infinitely conducting, ideal gas in which the dissipating processes are negligible. At the top of Figure 21 is a conceptual drawing of the interplanetary plasma and magnetic field parameters as function of (increasing) time. The parameters $\mathbf{V}_1$, N_1, and $\mathbf{B}_1$ characterize the interplanetary medium before the discontinuous jump in the parameters associated with the shock front. Following the time of the shock the parameters $\mathbf{V}_2$, N_2, and $\mathbf{B}_2$ characterize the interplanetary medium. In the lower section of Figure 21 is a drawing of the shock reference plane. Using the coordinate system defined in this figure the MHD shock jump conditions discussed above can be written as shown in Figure 22. For the purpose of these calculations the solar wind is assumed to consist only of protons and electrons and charge neutrality is assumed

$$\left[\rho v_x\right] = 0$$

$$\left[\rho v_x \hat{\vec{v}} + (P + B^2/2\mu)\hat{e}_x - \frac{B_x \vec{B}}{\mu}\right] = 0$$

$$\left[\rho v_x \left(\frac{P}{\gamma - 1} + \frac{v^2}{2} + \frac{B^2}{2\mu\rho}\right) + v_x \left(P + \frac{B^2}{2\mu}\right) - B_x \frac{\vec{B}\cdot\vec{v}}{\mu}\right] = 0$$

$$\left[\hat{\vec{v}} \times \hat{\vec{B}}\right]_y = 0$$

$$\left[\hat{\vec{v}} \times \hat{\vec{B}}\right]_z = 0$$

$$\left[B_x\right] = 0$$

Fig. 22. The magnetohydrodynamic shock jump conditions using the coordinate system defined in the shock reference plane drawing in Fig. 21.

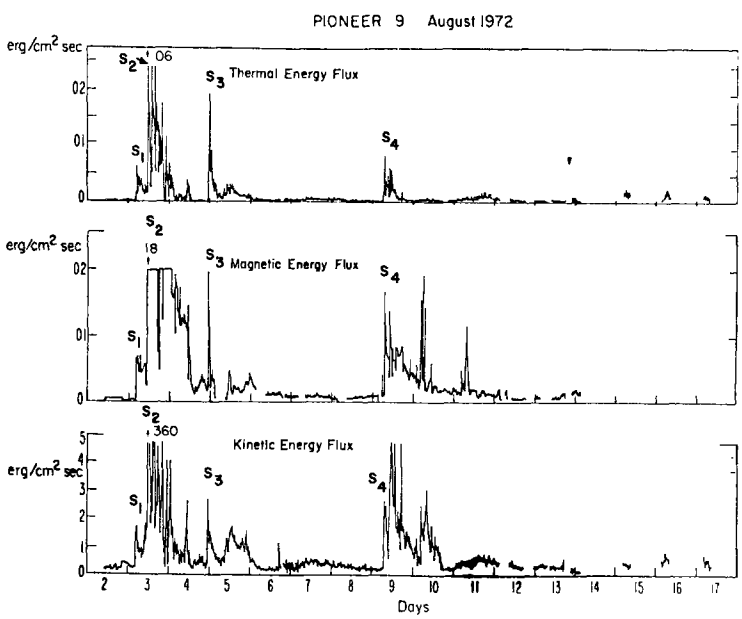

Fig. 23. The derived values of the kinetic energy flux, the magnetic energy flux, and the thermal energy flux obtained from the Rankine-Hugoniot analyses of Pioneer 9 data. The times of occurrence of the four forward shocks observed at Pioneer 9 are also indicated.

($n_e = n_p = n$). The plasma velocity, **v**, is measured in the shock reference frame so the top equation in Figure 22 is used to calculate the shock velocity V_S in terms of the plasma velocity measured in the spacecraft coordinate system, **u** (Dryer *et al.*, 1975b). For the four forward shocks seen at Pioneer 9 Dryer *et al.* (1976) have performed a three-dimensional least squares fitting of the simultaneous plasma and magnetic field data to the MHD shock conservation requirements shown in Figure 22. Using this analysis they have calculated the kinetic energy flux, the magnetic energy flux and the thermal energy flux in the interplanetary medium in early August 1972 based on the measurements at Pioneer 9. In Figure 23 which is adapted from Dryer *et al.* (1976), we have inserted information on the times of the four forward shocks $S_1(9)$, $S_2(9)$, $S_3(9)$, and $S_4(9)$. Dryer *et al.* (1976) have taken the kinetic energy flux to be homogeneous over a surface area at 0.78 AU subtended by 2π ster centered at the Sun (this assumption was made on the basis of the large volume indicated by the observations of the August 7th flare by Pioneer 9 and the interplanetary scintillation observations).

7. Shock Speeds

Dryer *et al.* (1976) using the method described above have also obtained the local velocities of the shocks at Pioneer 9. These results are also included in Table II. Recently a series of calculations have been carried out by Intriligator (1976a) and Smith (1976) to estimate the inertial speed of the shocks seen at Pioneer 9 and Pioneer 10 in association with the August events. These calculations are based on the assumption that the shocks are quasi-perpendicular. Then the conservation of magnetic flux leads to the relation for the inertial speed of the shock

$$V_{\text{Shock}}\langle V, B\rangle = \frac{V_2 B_2 - V_1 B_1}{B_2 - B_1} \tag{1}$$

where (as in the top drawing in Figure 21) V_1 and V_2 are, respectively, the values of the solar wind speed before and after the shock and B_1 and B_2 are, respectively, the values of the magnetic field magnitude before and after the shock. Table III, taken from Intriligator (1976a) lists the shock speeds found from this relation for each of the shocks observed at Pioneer 9. The shock speeds found from this relation for each of the shocks observed at Pioneer 10 are listed in Table IV. In Intriligator (1976a) there is also a discussion of the uncertainties associated with the calculated shock speeds shown in Table III and Table IV.

Intriligator (1976a) has also noted that shock speeds remarkably similar to those shown in Table III and Table IV are also obtained for each of the respective shocks at Pioneer 9 and Pioneer 10 when the shock speed is calculated using the equation

$$V_{\text{Shock}}\langle V, N\rangle = \frac{V_2 N_{p_2} - V_1 N_{p_1}}{N_{p_2} - N_{p_1}} \tag{2}$$

where (as in the top drawing of Figure 21) V_1 and V_2 are, respectively, the values of the

TABLE III

Local shock speeds at Pioneer 9 using Equation (1)

Event	Day	Time (UT)	V_1 (km s^{-1})	B_1 (gamma)	V_2 (km s^{-1})	B_2 (gamma)	$V_{Shock}\langle V, B\rangle$ (km s^{-1})
$S_1(9)$	D 216 (3 Aug.)	0420	297	1.5	345	4	374
$S_2(9)$	D 216 (3 Aug.)	1117	358	20	540	70	613
$S_3(9)$	D 217 (4 Aug.)	2323	685	9	938	23	1100
$S_4(9)$	D 222 (9 Aug.)	0707	403	8	546	18	660

TABLE IV

Local shock speeds at Pioneer 10 using Equation (1)

Event	Day	Time (UT)	V_1 (km s^{-1})	B_1 (gamma)	V_2 (km s^{-1})	B_2 (gamma)	$V_{Shock}\langle V, B\rangle$ (km s^{-1})
$S_1(10)$	D 219 (6 Aug.)	1520	412	2.5	615	7.5	717
$S_2(10)$	D 222 (9 Aug.)	1540	592	5	631	3	534
$S_3(10)$	D 226 (13 Aug.)	0300	502	1.2	605	3.5	659

solar wind speed before and after the shock; and N_{p_1} and N_{p_2} are, respectively the solar wind proton number densities before and after the shock. The results from estimating the shock speeds at Pioneer 9 and Pioneer 10 using this equation are shown in Table V and Table VI, respectively.

In Table VII (from Intriligator, 1976a) there is a comparison of the shock speeds obtained by these three different methods for each of the fast forward shocks at Pioneer 9. In the column $V_{Shock}\langle V, B\rangle$ the shock speeds are listed (as in the last

TABLE V

Local shock speeds at Pioneer 9 using Equation (2)

Event	Day	Time (UT)	V_1 (km s^{-1})	N_{p1} (protons cm^{-3})	V_2 (km s^{-1})	N_{p2} (protons cm^{-3})	$V_{Shock}\langle V, N_p\rangle$ (km s^{-1})
$S_1(9)$	D 216) (3 Aug.)	0420	297	6.3	345	14.2	383
$S_2(9)$	D 216 (3 Aug.)	1117	358	18	540	111	575
$S_3(9)$	D 217 (4 Aug.)	2323	685	0.7	938	1.4	1191
$S_4(9)$	D 222 (9 Aug.)	0707	403	2.5	546	7.2	622

TABLE VI

Local shock speeds at Pioneer 10 using Equation (2)

Event	Day	Time (UT)	V_1 (km s^{-1})	N_{p_1} (proton cm^{-3})	V_2 (km s^{-1})	N_{p_2} (proton cm^{-3})	$V_{\text{Shock}}\langle V, N_p\rangle$ (km s^{-1})
$S_1(10)$	D 219 (6 Aug.)	1520	412	1.6	615	5.1	708
$S_2(10)$	D 222 (9 Aug.)	1540	592	1.2	631	0.4	573
$S_3(10)$	D 226 (13 Aug.)	0300	502	0.4	605	1.0	674

TABLE VII

Comparison of calculated shock speeds at Pioneer 9

Event	Day	Time (UT)	$V_{\text{Shock}}\langle V, B\rangle$ (km s^{-1})	$V_{\text{Shock}}\langle V, N\rangle$ (km s^{-1})	$V_{SR(\text{Dryer})}$ (km s^{-1})
$S_1(9)$	D 216 (3 Aug.)	0420	374	383	431
$S_2(9)$	D 216 (3 Aug.)	1117	613	575	667
$S_3(9)$	D 217 (4 Aug.)	2323	1100	1191	1183
$S_4(9)$	D 222 (9 Aug.)	0707	660	622	672

column of Table III) from the calculations above (Equation (1)) assuming that the shocks are quasi-perpendicular. In the column $V_{\text{Shock}}\langle V, N\rangle$ the shock speeds are estimated (with Equation (2)) using the solar wind speed and the solar wind proton number density (as in the last column of Table V). The last column in Table VII lists the radial shock speeds, $V_{SR(\text{Dryer})}$ calculated by Dryer *et al.* (1976) (as in Table II) using the Rankine-Hugoniot relations. It should be noted that as discussed in Section 3, previously, e.g., Mihalov *et al.* (1972); Dryer *et al.* (1975a, 1976) the time of the first shock at Pioneer 9, $S_1(9)$, was incorrectly identified as $\sim$0440 UT. Intriligator (1976a) suggested the earlier ($<$0430 UT) identification and the shock speeds $V_{\text{Shock}}\langle V, B\rangle$ for $S_1(9)$ and $V_{\text{Shock}}\langle V, N\rangle$ for $S_1(9)$ are based on assuming that $S_1(9)$ occurred at $\sim$0420 UT whereas the calculation of the radial shock speed $V_{SR(\text{Dryer})}$ employs the 0440 UT identification.

Generally, the shock speeds $V_{\text{Shock}}\langle V, B\rangle$ calculated by Equation (1) assuming that the shocks are quasi-perpendicular agree quite well (within $\pm \lesssim 10\%$) with the $V_{SR(\text{Dryer})}$ calculated by Dryer *et al.* (1976) using the Rankine-Hugoniot relations. Even the shock speeds $V_{\text{Shock}}\langle V, N\rangle$ calculated using Equation (2) agree quite well with the others. For $S_2(9)$, using Equation (2) one obtains $V_{\text{Shock}}\langle V, N\rangle$ of 575 km s^{-1}.

Intriligator (1976a) has noted that Mihalov *et al.* (1974) calculated a shock speed of ~ 645 km s^{-1} for $S_2(9)$ using

$$V_S = \frac{N_{p_2} V_2 - N_{p_1} V_1}{N_{p_2} - N_{p_1}} \hat{n}$$

where $\hat{n}$ the best-fit shock normal was $\hat{n} = (-0.938, 0.341, 0.064)$. However, the Pioneer 9 number densities and other parameters used by Mihalov *et al.* (1974), were preliminary (as indicated in their note added in proof) and their subsequent analyses have led to the revision of these parameters to the values in Dryer *et al.* (1976).

To date no Rankine-Hugoniot analysis has been performed for the Pioneer 10 data but Intriligator (1976a) has compared the shock speeds obtained at Pioneer 10 using Equation (1) with those obtained using Equation (2). This comparison is summarized in Table VIII. There is a very good agreement ($\pm \lesssim 10\%$) between the calculated shock speeds at Pioneer 10.

TABLE VIII

Comparison of calculated shock speeds at Pioneer 10

Event	Day	Time (UT)	$V_{\text{Shock}}\langle V, B\rangle$ (km s^{-1})	$V_{\text{Shock}}\langle V, N\rangle$ (km s^{-1})
$S_1(10)$	D 219 (6 Aug.)	1520	717	708
$S_2(10)$	D 222 (9 Aug.)	1540	534	573
$S_3(10)$	D 226 (13 Aug.)	0300	659	674

8. Pioneer 9/Pioneer 10 Shock Associations

Recently, Intriligator (1976a) and Smith (1976) have pointed out the similarity of the shock speeds calculated for $S_2(9)$ and $S_1(10)$ and have compared these shock speeds with the estimated average velocity of the shock obtained by assuming that the shock $S_2(9)$ propagated radially outward from Pioneer 9 to Pioneer 10 where it is identified as $S_1(10)$. This leads to an estimated average shock speed of ~ 770 km s^{-1}. The agreement between this average shock speed with the local shock speeds $S_2(9)$ and $S_1(10)$ have led Intriligator (1976a) and Smith (1976) to conclude that the previous association by others between $S_3(9)$ and $S_1(10)$ was incorrect. This conclusion appears to be further supported by the HEOS-2 data obtained near Earth. Cattaneo *et al.* (1974) have calculated that the shock speed of $S_2(E)$ was on the order of 730 km s^{-1}.

The association of $S_2(9)$ and $S_1(10)$ is also important (Intriligator, 1976a; Smith, 1976) because it leads one to the conclusion that there was no strong deceleration of the shock as it propagated outward from Pioneer 9 at 0.78 AU to Pioneer 10 at 2.2 AU. This conclusion is emphasized in the top section of Figure 24 from Intriligator (1976a). In this figure the local shock speeds $V_{SR(\text{Dryer})}$ and $V_S\langle V, B\rangle$ at Pioneer 9

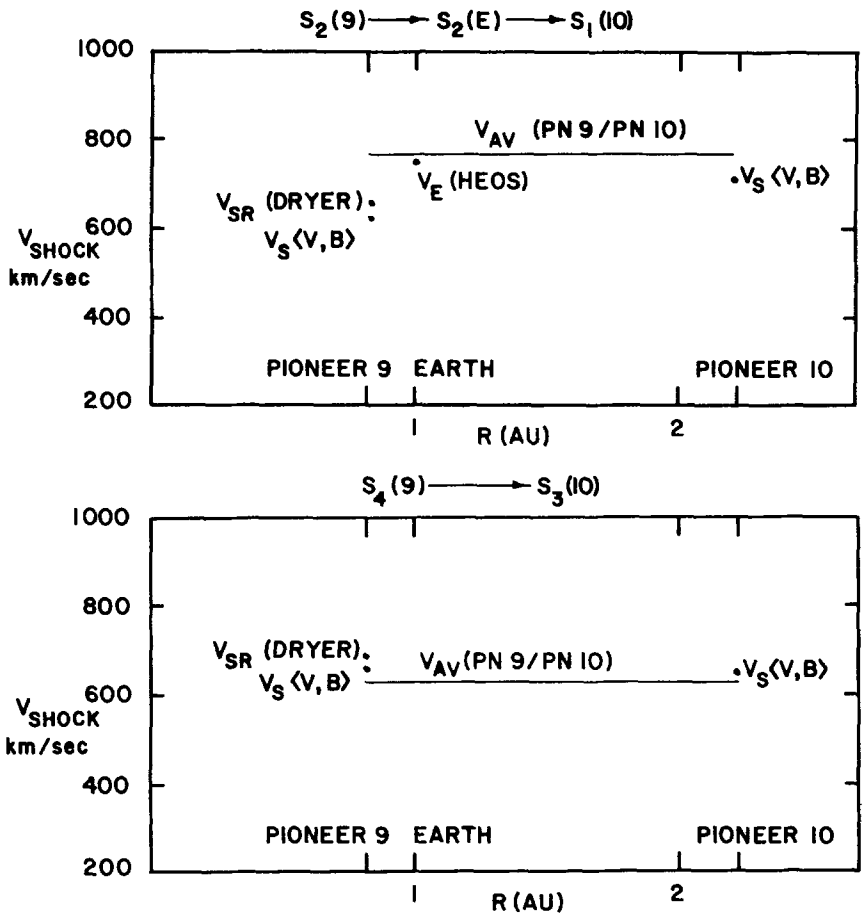

Fig. 24. (upper panel). Summary of local shock speeds obtained (see text) for the forward shocks $S_2(9)$, $S_2(E)$, and $S_1(10)$ and the average shock speed V_{AV}(Pn 9/Pn 10) implied (see text) by associating $S_2(9)$ with $S_1(10)$. This figure emphasizes the similarity of each of these speeds and implies that the fast forward shock $S_2(9)$ propagated between 0.8 AU and 2.2 AU without strongly decelerating. (Lower panel) Summary of local shock speeds obtained (see text) for the forward shocks $S_4(9)$ and $S_3(10)$ and the average shock speed V_{AV}(Pn 9/Pn 10) implied (see text) by associating $S_4(9)$ with $S_3(10)$. This figure also emphasizes the similarity of each of these speeds and implies that the fast forward shock $S_4(9)$ propagated between 0.8 AU and 2.2 AU without strongly decelerating.

are shown, the shock speed $V_{S(\mathrm{HEOS})}$ of ~ 730 km s^{-1} calculated near Earth by Cattaneo *et al.* (1974) is shown, the local shock speed $V_S\langle V, B\rangle$ at Pioneer 10 is indicated. The line V_{AV}(Pn 9/Pn 10) represents the estimated average shock speed (~ 770 km s^{-1}) based on the elapsed time of observation between $S_2(9)$ and $S_1(10)$ at Pioneer 9 and Pioneer 10, respectively. It is evident in the top section of Figure 24 that all of these speeds are similar and that contrary to some theoretical expectations and earlier reports there is no evidence between ~ 0.8 AU and 2.2 AU for a strong deceleration of the shock with increasing heliocentric distance.

In Figure 25 (from Intriligator, 1976a) the shock associations are summarized.

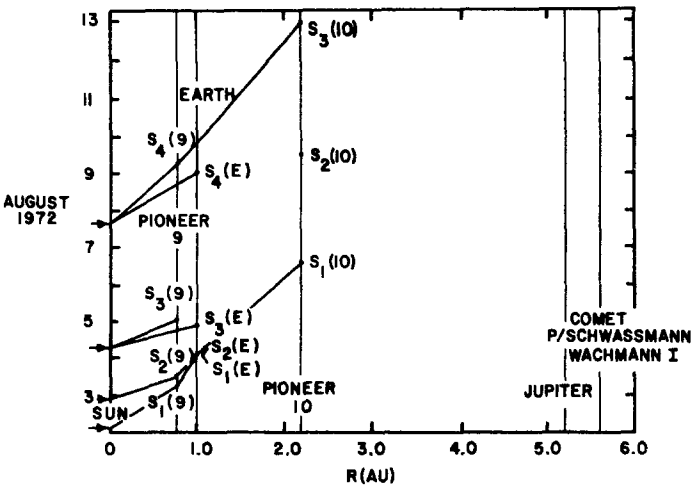

Fig. 25. Summary of flare and shock associations based upon the analyses of local shock speeds. The times of the four flares (see Table I) are indicated at the left by arrows. The dots indicate the times of arrival of the shocks at Pioneer 9, Earth, and Pioneer 10. The straight lines connecting the dots indicate the shock associations at the various sites of observation.

$S_1(9)$ was overtaken beyond 1 AU by $S_2(9)$ which propagated outward to become $S_1(10)$ (as indicated in Figure 24 $S_1(9)$ is identified with $S_1(E)$ at Earth and $S_2(9)$ is identified with $S_2(E)$ at Earth).

A comparison of the estimated shock speeds for $S_4(9)$ in Table VII with the estimated shock speeds for $S_3(10)$ in Table VIII points out the similarity between these two local shock speeds. Intriligator (1976a) and Smith (1976) have identified $S_4(9)$ at Pioneer 9 with $S_3(10)$ at Pioneer 10 and then on this basis have each estimated an average speed of ~ 635 km s^{-1} for the propagation from Pioneer 9 to Pioneer 10. In Figure 25 the shock identification of $S_4(9)$ at Pioneer 9 with $S_3(10)$ at Pioneer 10 is clearly indicated. In the lower section of Figure 24 this average estimated speed V_{AV}(Pn 9/Pn 10) and the local shock speeds at Pioneer 9 and Pioneer 10 are shown. As in the case of the association of $S_2(9)$ and $S_1(10)$ discussed above, it is evident in this figure that all of the speeds are similar. Therefore, the identification of $S_4(9)$ and $S_3(10)$ and a comparison of their local shock speeds leads to the conclusion (Intriligator, 1976a; Smith, 1976) that in this case also there was no strong deceleration of the shocks between Pioneer 9 at ~ 0.8 AU and Pioneer 10 at ~ 2.2 AU.

9. Estimates of Shock Thickness

Using the local shock speeds calculated above and the high resolution magnetic field data, Intriligator (1976a) and Smith (1976) have estimated the shock thickness for $S_1(10)$ the first forward shock observed at Pioneer 10 and for $S_2(10)$ the reverse shock observed at Pioneer 10. The data gap at the time of $S_3(10)$ precludes the calculation of the shock thickness for this forward shock. For $S_1(10)$, using $V_{\text{Shock}}\langle V, B\rangle \sim 717$ km s^{-1}

and $\Delta t \sim 2$ s they obtain $\Delta L \sim 1400$ to 1500 km. For $S_2(10)$ using $V_{\text{Shock}}\langle V, B\rangle \sim$ 534 km s^{-1}, and $\Delta t \lesssim 1$ s they obtain $\Delta L \sim 500$ to 600 km. Intriligator (1976a) and Smith (1976) have noted that these shock thicknesses are larger than the comparable c/ω_{pi}, the ion inertial length.

The thickness obtained here for $S_1(10)$ is substantially less than the upper limit for $S_2(9)$ for 11.6×10^4 km reported by Dryer *et al.* (1976). In general the estimates of Dryer *et al.* (1976) appear quite high (Intriligator, 1976a). Using the reported thickness of Dryer *et al.* (1976) for $S_2(9)$ and the local shock speed $V_{\text{Shock}}\langle V, B\rangle$ obtained above

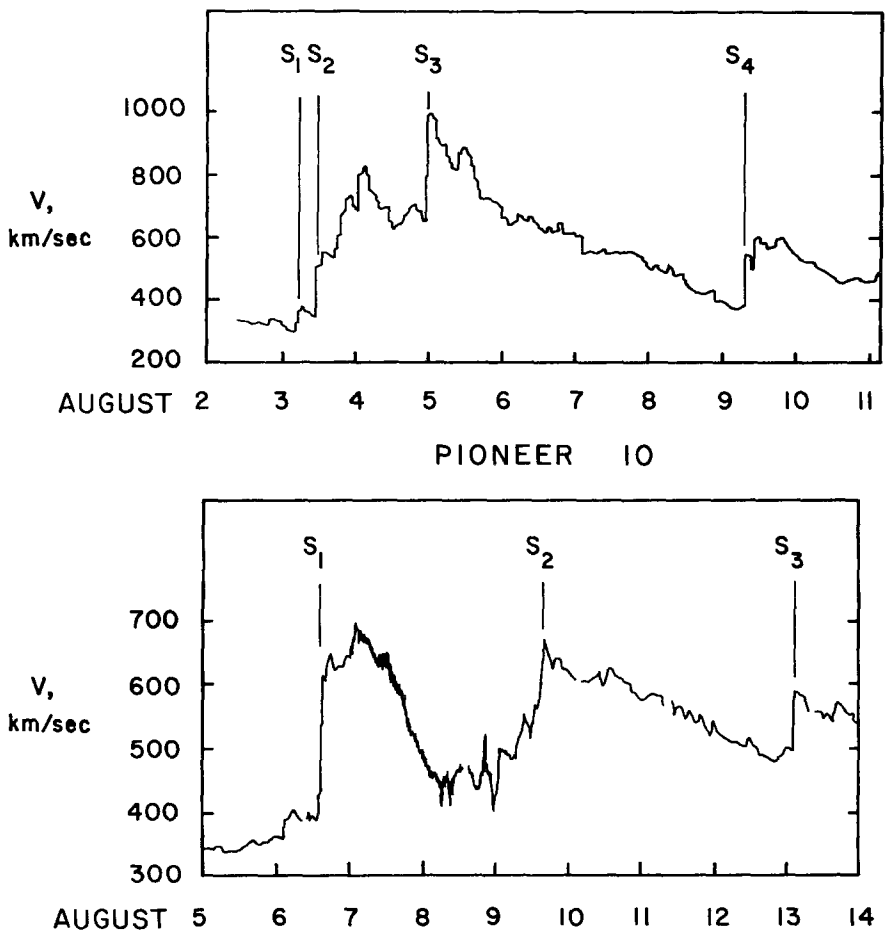

Fig. 26. Summary of the solar wind proton speed measurements obtained by Pioneer 9 (~0.8 AU) and Pioneer 10 (2.2 AU). The times of the four forward shocks observed at Pioneer 9 are indicated. Also shown are the times at Pioneer 10 of the two forward shocks $S_1(10)$ and $S_3(10)$ and the one reverse, shock $S_2(10)$. The obvious decrease in the speed following $S_1(10)$ in contrast to the generally higher levels following $S_2(9)$ is shown.

of ~ 613 km s^{-1}, Intriligator (1976a) shows that this implies a $\Delta t \sim 3$ min (~ 189 s). Even if the shock thicknesses at Pioneer 9 were on the order of ~ 500 km to 1600 km as is the case at Pioneer 10, they would still be substantially larger than their respective ion inertial lengths (see Table II).

10. Other Analyses

In Figure 26 the Pioneer 9 and Pioneer 10 measurements of the solar wind proton streaming speed are summarized and the shocks $S_1(9)$, $S_2(9)$, $S_3(9)$, $S_4(9)$ and $S_1(10)$, $S_2(10)$, and $S_3(10)$ are indicated. Mihalov *et al.* (1974) and others, e.g., Intriligator (1976a, b), Scarf and Wolfe (1974) have noted the general change in the profiles of the solar wind speed. The most obvious change is the decrease in the speed following $S_1(10)$ in contrast to the generally higher levels following $S_2(9)$. In contrast the solar wind temperatures measured at Pioneer 10 following $S_1(10)$ are higher than those expected for a pure adiabatic expansion of the solar wind. The elevated temperatures at Pioneer 10 could be attributed to stream/stream interactions and/or to the systematic conversion of the (directed) streaming speed into the (random) temperature. This systematic conversion could be the result of the growth of turbulence in the interplanetary medium and/or the result of plasma/wave interactions and plasma instabilities.

Scarf and Wolfe (1974) have studied the Pioneer 9 plasma wave and plasma measurements and reported that enhanced wave levels were detected over extended time periods associated with the August events. Figure 27, taken from Scarf and Wolfe (1974) is a wave level/proton density scatter plot for the time period of the August events. The plot contains all pairs of measurements made with a time separation of 1 min or less. Scarf and Wolfe (1974) note that the in-flight threshold levels for the broad band channel were measured whenever the density was low. The vertical dashed line in the lower left side of the figure indicates the lowest proton density for which the ion acoustic wave dispersion relation

$$\left(\frac{1}{\omega^2} \simeq \frac{M_i}{k^2 k T_e} + \frac{1}{\omega_p^i} + \cdots\right)$$

gives a solar wind rest frame frequency equal to the channel cutoff at 100 Hz. Scarf and Wolfe (1974) concluded that the data in this figure are consistent with the use of the ion acoustic wave dispersion relation in the solar wind frame of reference. Scarf and Wolfe (1974) also speculate on the magnitude of a numerically small average Doppler shift ($\langle \Delta f/f \rangle \lesssim 0.2$) for ($\mathbf{k} \cdot \mathbf{V}$) combinations that yield f(wind) $< f$(Pioneer 9).

Recently Intriligator (1976b) has estimated power spectra (Intriligator, 1975a, b) of the solar wind proton streaming speed measured at Pioneer 9 and Pioneer 10. The results indicate that the time series analyses and the power spectral analyses of the data from both spacecraft are consistent and may imply that as the interplanetary disturbance $S_1(9)$, $S_2(9)$ propagates outward there may be a conversion of the (directed)

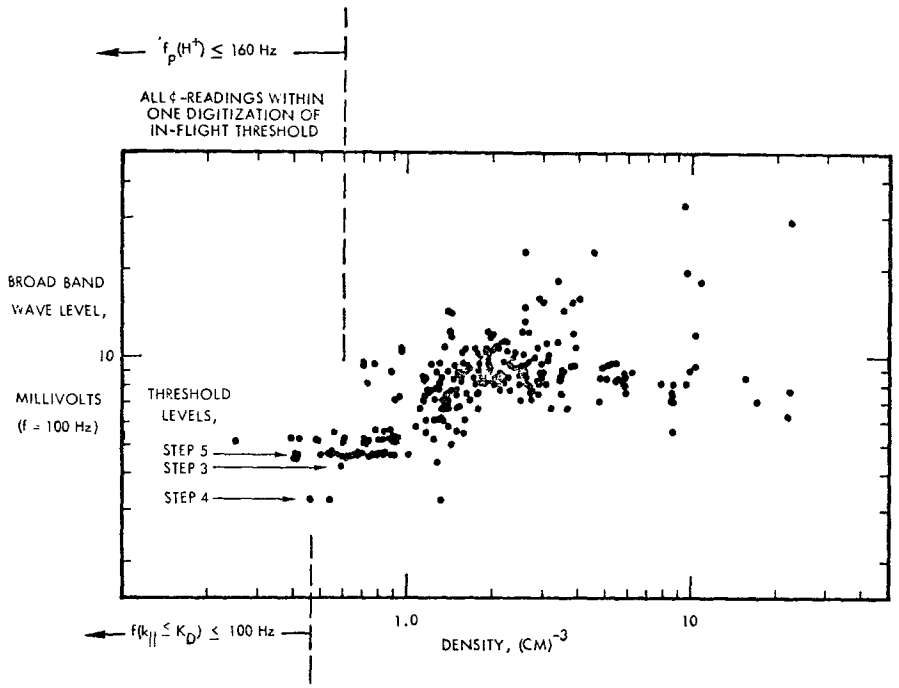

Fig. 27. Pioneer 9 wave level/proton density scatter plot for the time period associated with the August events. This figure contains all measurements made with a time separation of 1 minute or less. In-flight threshold levels for the broadband channel were measured whenever the density was low. The vertical dashed line in the lower left indicates the lowest proton density for which the ion acoustic wave dispersion relation (see text) gives a solar wind rest frame frequency equal to the channel cutoff at 100 Hz.

streaming energy of the solar wind protons into the (randomized) thermal heating of the solar wind protons. The power spectral analyses of the solar wind proton streaming speed are in the 10^{-4}–10^{-2} Hz frequency range (Intriligator, 1975a, b). The interplanetary scintillation of radio sources (Jokipii, 1973) is a useful probe for indirectly measuring the fluctuations in the solar wind electron density at higher frequencies. The interplanetary scintillation of radio sources can also be used to probe in regions of the solar system currently not accessible to spacecraft (e.g., out of the ecliptic). There is a detailed review of the interplanetary scintillation observations associated with the August events in Kakinama and Watanabe (1976).

11. Summary

We have reviewed many of the interplanetary features associated with the solar flares in August 1972. It is anticipated that future studies of these interplanetary features will reveal additional information that will enable us to further understand the solar wind dynamics associated with these events. In addition, as a result of the recent Pioneer 10 and Pioneer 11 direct exploration of the solar system to extended helio-

centric distances (to date as great as 10 AU), there have been some important studies (e.g., Smith and Wolfe, 1976) of the interaction between adjacent solar wind streams at large heliocentric distances. It is anticipated that future studies of this kind and computer simulations of solar wind phenomena out to large heliocentric distances (e.g., Dryer *et al.*, 1976; Dryer and Steinolfson, 1976), and laboratory experiments may also enable us to more fully understand the solar wind dynamics associated with the August events and other solar wind phenomena at large heliocentric distances.

Acknowledgments

The author is indebted to J. H. Wolfe, E. J. Smith, C. P. Sonett, and D. S. Colburn for the use of their Pioneer data and to J. H. Wolfe, J. D. Mihalov, E. J. Smith, and M. Dryer for many helpful discussions. This work was supported by the National Aeronautics and Space Administration under Contract NAS2-7969 and Grant NGR 05-018-181, and the University of Southern California.

References

Cattaneo, M. B., Cerulli-Irelli, P., Diodato, L., Egidi, A., Moreno, G., and Hedgecock, P. C.: 1974, in D. E. Page (ed.), *Correlated Interplanetary and Magnetospheric Observations*, D. Reidel Publ. Co., Dordrecht, Holland, p. 555.

Colburn, D. S. and Sonett, C. P.: 1966, *Space Sci. Rev.* **5**, 439.

Croft, T. A.: 1975, preprint.

Dryer, M., Eviatar, A., Frohlich, A., Jacobs, A., Joseph, J. H., and Weber, E. J.: 1975a, *J. Geophys. Res.* **80**, 2001.

Dryer, M., Smith, Z. K., Unti, T., Mihalov, J. D., Smith, B. F., Wolfe, J. H., Colburn, D. S., and Sonett, C. P.: 1975b, *J. Geophys. Res.* **80**, 3225.

Dryer, M., Smith, Z. K., Steinolfson, R. S., Mihalov, J. D., Wolfe, J. H., and Chao, J. K.: 1976, *J. Geophys. Res.* **81** (in press).

Dryer, M. and Steinolfson, R. S.: 1976, preprint.

Intriligator, D. S.: 1973, preprint.

Intriligator, D. S.: 1975a, *Astrophys. J.* **196**, L87

Intriligator, D. S.: 1975b, *Astrophys. J.* **196**, 879.

Intriligator, D. S.: 1976a, *J. Geophys. Res.* (in press).

Intriligator, D. S.: 1976b, preprint.

Intriligator, D. S. and Neugebauer, M.: 1975, *J. Geophys. Res.* **80**, 1332.

Intriligator, D. S. and Wolfe, J. H.: 1976, in T. Gehrels (ed.), *Jupiter*, University of Arizona Press, Tucson, Arizona, p. 848.

Jokipii, J. R.: 1973, *Ann. Rev. Astron. Astrophys.* **11**, 1.

Kakinuma, T. and Watanabe, T.: 1976, *Space Sci. Rev.*, this issue.

Landau, L. D. and Lifshitz, E. M.: 1960, *Fluid Mechanics*, Addison-Wesley Publ. Co., Reading, Mass.

Lepping, R. P. and Argentiero, P. D.: 1971, *J. Geophys. Res.* **76**, 4349.

Mihalov, J. D., Colburn, D. S., Collard, H. P., Smith, B. F., Sonett, C. P., and Wolfe, J. H.: 1974, in D. E. Page (ed.), *Correlated Interplanetary and Magnetospheric Observations*, D. Reidel Publ. Co., Dordrecht, Holland, p. 545.

Scarf, F. L. and Wolfe, J. H.: 1974, *J. Geophys. Res.* **79**, 4179.

Smith, E. J.: 1976, this issue, p. 661.

Smith, E. J., Davis, L., Jr., Jones, D. E., Coleman, P. J., Jr., Colburn, D. S., Dyal, P., Sonett, C. P., and Frandsen, A. M. A.: 1974, *J. Geophys. Res.* **79**, 3501.

Smith, E. J. and Wolfe, J. H.: 1976, *Geophys. Res. Lett.* **3**, 137.
Tidman, D. A. and Krall, N. A.: 1971, *Shock Waves in Collision-less Plasmas*, Wiley-Interscience, New York, pp. 7–18.
Vaisberg, O. L. and Zastenker, G. N.: 1976, this issue, p. 687.
World Data Center A for Solar Terrestrial Physics: 1973, Collected Data Reports on August 1972, Solar-Terrestrial Events, *UAG-28*, Boulder, Colorado.
Zastenker, G. N., Vaisberg, O. L., Cambou, F., Temnyi, V. V., and Khokhlov, M. Z.: 1975, Preprint D-188, Space Res. Instit. Acad. Sci. U.S.S.R., presented at COSPAR Meeting, Varna, Bulgaria, 2–7 June.